Integrated state and parameter estimation for vehicle dynamics control

Article *in* International Journal of Vehicle Performance · January 2019

DOI: 10.1504/IJVP.2019.10025783

2 authors:

Saied Taheri
Virginia Tech (Virginia Polytechnic Institute and State University)
124 PUBLICATIONS **1,658** CITATIONS
SEE PROFILE

Kanwar Bharat Singh
Goodyear
28 PUBLICATIONS **519** CITATIONS
SEE PROFILE

Integrated state and parameter estimation for vehicle dynamics control

Kanwar Bharat Singh*

Department of Tire Vehicle Mechanics,
The Goodyear Tire and Rubber Company,
L-7750, Avenue Gordon Smith,
Colmar-Berg, Luxembourg
Email: kanwar-bharat_singh@goodyear.com
*Corresponding author

Saied Taheri

Department of Mechanical Engineering,
Virginia Tech,
332 Randolph Hall,
Blacksburg, VA 24061, USA
Email: staheri@vt.edu

Abstract: Most modern day automotive chassis control systems employ a feedback control structure. Therefore, a real-time estimate of the vehicle handling dynamic states and tyre-road contact parameters are invaluable for enhancing the performance of current vehicle control systems, such as anti-lock brake system (ABS) and electronic stability program (ESP). Today's production cars are equipped with onboard sensors (e.g., a 3-axis accelerometer, 3-axis gyroscope, steering wheel angle sensor, and wheel speed sensors) which when used in conjunction with certain model based observers can be used to identify relevant vehicle states for optimal control of comfort, stability and handling. However, some key variables such as the tyre forces, road bank/grade angles, and the tyre-road friction coefficient, which have a significant impact on vehicle handling performance and safety are difficult to measure using sensors already onboard vehicles. This paper introduces an integrated vehicle state estimator comprising a series of model-based and kinematic-based observers for estimating these unmeasurable states. Using an appropriate vehicle model, kinematic equations of motion and vehicle sensor data, the unknown vehicle states as well as the tyre-road contact forces are estimated by implementing a series of observers arranged in a cascade structure. Key estimated signals include the vehicle side slip angle (β), tyre longitudinal/lateral/vertical forces, and the tyre-road friction coefficient (μ). The performance of the proposed estimators has been evaluated via computer simulations conducted using the vehicle dynamics software CarSim®. An effectively designed merging scheme ensures robust estimation performance even during the vehicle manoeuvres which show highly nonlinear tyre characteristics and in the existence of road inclination or bank angle.

Keywords: state estimation; parameter estimation; SMO; sliding mode observer; KF; Kalman filter; RLS; recursive least squares.

Reference to this paper should be made as follows: Singh, K.B. and Taheri, S. (2019) 'Integrated state and parameter estimation for vehicle dynamics control', *Int. J. Vehicle Performance*, Vol. 5, No. 4, pp.329–376.

Biographical notes: Kanwar Bharat Singh received his Master's degree in Mechanical Engineering from Virginia Tech, USA in 2012. Since 2012, he has been working as a Senior Research Engineer at the Goodyear Innovation Center. He holds several US patents and has authored numerous peer reviewed technical papers in reputed journals. His current research interests include intelligent tyres, vehicle state estimation and machine learning for automotive applications.

Saied Taheri is the Cofounder and the Director of the Center for Tyre Research (CenTiRe) at Virginia Tech. He had worked at Ford Motor Company, Tehran Polytechnic Institute, TRW Automotive, and Goodyear Tyre and Rubber Company prior to joining Virginia Tech in 2007 where he is currently a Professor in Mechanical Engineering Department. He has published more than 150 journal and conference papers.

1 Introduction

For implementation of automotive control algorithms, accurate information about the state of the vehicle and its surroundings is important. Real-time measurements of the vehicle handling dynamic states are extremely vital for the online computation of the optimised active longitudinal and lateral tyre forces to be generated by electronic stability control modules. Although some of these states are easily measured, others are difficult to measure because of high cost or impracticality. Therefore, vehicle-control systems currently available on production cars rely on available inexpensive measurements, such as wheel speeds, accelerations and yaw-rate. Knowledge about additional states of a vehicle (e.g., vehicle roll angle, side slip angle, lateral load transfer ratio etc.) can significantly reduce the risk of accidents through effective design and implementation of advanced chassis control systems. As a result, the problem of vehicle state estimation has attracted considerable attention of many researchers and many studies have been conducted to estimate vehicle states using model based and/or kinematic based estimation techniques.

A *summary* description of the *state-of-the-art* in the field of vehicle state estimation is given in Table 1. In works by Baffet et al. (2008, 2009) and Zhang et al. (2009), a sliding mode observer is proposed to estimate tyre-road forces, while an extended Kalman filter estimates sideslip angle and cornering stiffness. An extended Kalman filter based estimation process for lateral load transfer and wheel-ground contact normal forces is developed in Doumiati et al. (2008, 2009a, 2009d). In Fathy et al. (2008), Vahidi et al. (2005), a recursive least square scheme for the online estimation of vehicle mass is examined. Cho et al. (2010) presents a scheme for longitudinal/lateral tyre-force estimation using a random-walk Kalman filter. Doumiati et al. (2009b, 2009c, 2010a, 2010b, 2011), two observers derived from extended and unscented Kalman filtering techniques are proposed and compared to estimate tyre-road forces and vehicle sideslip angle. A method for the evaluation of a risk skid indicator based on the estimation of the maximum friction coefficient is proposed in (Ghandour et al., 2010, 2011a, 2011b).

Doumiati et al. (2011a) present a method to estimate the road profile elevation based on a classical Kalman filter. Grip et al. (2009b) presents a nonlinear vehicle sideslip observer with reduced computational complexity compared to an extended Kalman filter. In Ray (1995) and Samadi et al. (2001), an extended Kalman filter based method is presented to estimate the dynamic state and tyre-road forces for a nonlinear vehicle model. In Rabhi et al. (2007) and M'sirdi et al. (2006) cascaded observers based on first or second order sliding modes are used to estimate the contact forces. Hsiao et al. (2011) presents a tyre force estimator, designed by accounting for the dependency between the longitudinal and lateral tyre forces by introducing the friction ellipse into the estimation algorithm. In Dakhlallah et al. (2008) and Sebsadji et al. (2008), an extended Kalman filter and Luenberger observer based method for the estimation of the vehicle dynamics using a nonlinear vehicle model is proposed. In Zhu and Zheng (2008), Pan et al. (2009), Chen and Hsieh (2008) and Cheng et al. (2011), a nonlinear observer using unscented Kalman filter (UKF) to estimate sideslip angle is presented. In Nam et al. (2011), lateral tyre forces obtained from a multi-sensing hub unit are used to estimate vehicle lateral velocity and roll angle using a recursive least square algorithm and a Kalman filter. Hu et al. (2010) and Chu et al. (2010) present a vehicle lateral and longitudinal velocity estimation method using an adaptive/unscented Kalman filter. In Tanelli et al. (2006), an algorithm for the estimation of longitudinal vehicle speed, based on the measurements of the four-wheel rotational speeds and of the longitudinal vehicle acceleration is presented. In Chu et al. (2011), a fuzzy logic is used to get an estimate of the vehicle longitudinal velocity; together with the estimated vehicle longitudinal acceleration, a Kalman filter is used to estimate the velocity of vehicle for use in ESC control applications. Chen et al. (2010) and Ryu et al. (2007) present a Kalman filter based approach to estimate roll angle and roll rate with either a three-degree-of freedom (3DOF), or 1DOF vehicle model. In (Yi et al., 2007), an estimator design based on a three-degree-of-freedom vehicle manoeuvring model and a four-degree-of-freedom half-car suspension model is used to obtain estimates of the vehicle roll angle and roll rate in driving situations in which both manoeuvring and road disturbances affect the vehicle roll motions. In Hac et al. (2004), an approach using a closed-loop adaptive observer for estimating roll angle and roll rate of vehicle body with respect to the road is proposed. Works from Rajamani et al. (2009, 2011) focuses on algorithms to estimate roll angle and CoG height. The algorithms investigated include a sensor fusion algorithm that utilises a low frequency tilt angle sensor, a gyroscope and a dynamic observer that utilises only a lateral accelerometer and a gyroscope. In Tsourapas et al. (2009), two rollover indexes are proposed and analysed. The first rollover index estimates the actual lateral transfer ratio (LTR) while the second index referred to as the predictive lateral transfer ratio (PLTR), incorporates the predictive influence of the driver's steering input. Oh and Choi (2011) focus on the accurate estimation of the vehicle states, including the longitudinal, lateral, and vertical velocities, as well as the roll and pitch angles, using merging schemes that combine the kinematic and model-based observer outputs. In Tseng (2001), Eric Tseng et al. (2007) and Rehm (2010), methods for estimation of road inclination and bank angle are presented. In Grip et al. (2009a), a scheme for the vehicle roll angle is derived based on the combination of sensors from vehicle dynamics control system and a rollover mitigation system. In Cho et al. (2010) and Hac et al. (2010), methods for compensating the gravity components of the lateral acceleration are proposed. Hsu et al. (2010) present a model based estimation method that utilises pneumatic trail information in steering torque to identify a vehicle's lateral handling limits.

Table 1 State-of-the-art literature review

Measurements used	*Estimated states*	*Model used*	*Estimation methodology*	*References*
r, a_y, a_x, δ	Tyre forces and vehicle sideslip angle	Single-track model	SMO, EKF	Baffet et al. (2008, 2009), Zhang et al. (2009)
a_y, a_x, δ_{sus}	Tyre normal force	Vehicle roll dynamic model	EKF	Doumiati et al. (2008, 2009a, 2009d)
$a_x, v_x, r, \lambda, T_e, T_b$	Vehicle mass	Longitudinal dynamics	RLS	Fathy et al. (2008) and Vahidi et al. (2005)
$r, a_y, a_x, \delta, \omega_w, T_e, T_b$	Tyre forces	Wheel dynamics model, vehicle planar model	KF	Cho et al. (2010)
$a_y, a_x, \delta_{sus}, r, p, \delta, \omega$	Tyre forces and vehicle sideslip angle	Four-wheel vehicle model	EKF, UKF	Doumiati et al. (2009b, 2009c, 2010a, 2010b), Doumiati et al. (2011b)
$a_y, a_x, \delta_{sus}, r, p, \delta, \omega$	Tyre-road friction coefficient and vehicle lateral skid indicator	Four-wheel vehicle model	EKF, UKF, NLLS	Ghandour et al. (2010, 2011)
$a_y, a_x, \delta_{sus}, r, p, \delta, \omega$	LTR (Lateral load transfer) and LSI (Lateral skid indicator)-Accident risk prediction	Four-wheel vehicle model	EKF, UKF, NLLS	Ghandour et al. (2011)
a_y, δ_{sus}	Road profile and wheel load	Quarter-car model	KF	Doumiati et al. (2011)
r, a_y, a_x	Vehicle sideslip angle	Kinematics model	Nonlinear observer	Grip et al. (2009b)
r, a_y, a_x, ω	Tyre forces	Nonlinear vehicle model	EKF	Ray (1995), Samadi et al. (2001)

Table 1 State-of-the-art literature review (continued)

Measurements used	*Estimated states*	*Model used*	*Estimation methodology*	*References*
T_w, v_x, θ_w	Velocities and accelerations of the wheels, tyre forces (vertical and longitudinal) and friction coefficient	Wheel dynamics model	Robust differentiator and sliding modes	Rabhi et al. (2007) and M'sirdi et al. (2006)
T_w, ω, r, a_x, a_y	Tyre forces and vehicle parameter estimation	Wheel dynamics model, vehicle planar model, Friction ellipse	Model based	Hsiao et al. (2011)
$r, a_x, a_y, \omega, \delta$	Tyre forces and road grade	Four-wheel vehicle model	EKF, Luenberger observer	Dakhlallah et al. (2008) and Sebsadji et al. (2008)
a_x, a_y, ω, δ	Vehicle sideslip angle and yaw rate	Bicycle model	UKF	Zhu and Zheng, 2008) and Pan et al. (2009)
a_x, a_y, r	Vehicle sideslip angle	Kinematic model	EKF	Chen and Hsieh (2008)
a_x, a_y, v_x, δ, r	Vehicle sideslip angle, lateral tyre road forces and tyre road friction coefficient	Four-wheel vehicle model	UKF	Cheng et al. (2011)
F_y	Vehicle sideslip angle	Yaw plane model	RLS	Nam et al. (2011)
$r, a_x, a_y, \omega, \delta$	Vehicle longitudinal and lateral velocity	Bicycle model	AKF, UKF	Hu et al. (2010) and Chu et al. (2010)
a_x, ω	Vehicle longitudinal velocity	Kinematics-based	Rule Based	Tanelli et al. (2006)
a_x, ω	Vehicle longitudinal velocity	Yaw plane model	KF, Fuzzy logic	Chu et al. (2011)
a_y, p	Roll angle	Vehicle roll dynamic model	KF	Chen et al. (2010) and Ryu et al. (2007)

Table 1 State-of-the-art literature review (continued)

Measurements used	*Estimated states*	*Model used*	*Estimation methodology*	*References*
a_y, r, δ	Roll angle and roll rate	Lateral-dynamics-model a four-degree-of-freedom half-car suspension model	KF	Park et al. (2008) and Yi et al. (2007)
a_y, p	Roll angle	Vehicle roll dynamic model	Closed loop adaptive observer	Hac et al. (2004)
$a_y, p, \phi_{tilt\ angle\ sensor}$	Roll angle and center of gravity height	Kinematic sensor fusion, Vehicle roll dynamic model	Sensor fusion	Rajamani et al. (2009, 2011)
a_y, p	Load Transfer Ratio (LTR) and Predictive Load Transfer Ratio (PLTR)	Vehicle roll dynamic model	Model based	Tsourapas et al. (2009)
a_x, a_y, a_z, p, q, r	Roll and pitch angles, longitudinal, lateral, and vertical velocities	Kinematic and model-based (bicycle model) observer	Merging schemes	Oh and Choi (2011)
a_y, r, δ	Road bank angle	Bicycle model	Transfer function approach, *superposition*	Tseng (2001)
$a_x, a_y, p, q, r, \omega$	Vehicle roll and pitch angles	Kinematics-based observer	State observer	Tseng et al. (2007)
$r, a_x, a_y, \omega, \delta$	Road bank and grade angles	Kinematic model	*Observers* using *time-varying gains*	Rehm (2010)
p	Roll angle	Vehicle roll dynamic model	Controlled integration	Grip et al. (2009a)

Table 1 State-of-the-art literature review (continued)

Measurements used	*Estimated states*	*Model used*	*Estimation methodology*	*References*
a_y, r, v_x, p	Roll angle	Vehicle roll dynamic model, Kinematic model	Vehicle state index based switching	Cho et al. (2010)
$r, \omega, \delta, a_y, p$	Vehicle roll angle and Sideslip angle	Kinematic model	Weighting function	Hac et al. (2010)
r, δ, a_y, v_x	Tyre Slip angle	Bicycle model	State observer	Hsu et al. (2010)

*List of acronyms- SMO: Sliding mode observer, KF: Kalman Filter, EKF: Extended Kalman Filter, UKF: Unscented Kalman Filter, AKF: Adaptive Kalman Filter, RLS: Recursive least squares, NLLS: Nonlinear least squares.

Another research topic related to state estimation that has garnered considerable attention is the concept of system state estimation for active suspension control. This is driven by the need to develop more advanced control systems for semi-active and fully active suspension systems which are becoming more and more common on production vehicles. In Pletschen and Badur (2014), the concept of Takagi-Sugeno observer design has been adopted for nonlinear state estimation in an actively controlled vehicle suspension application. In Hernandez-Alcantara et al. (2014), an observer capable of estimating the unmeasured state variables of the quarter of vehicle (QoV) dynamics subject to unknown road surfaces is proposed. In Rath et al. (2014), an adaptive super-twisting observer was proposed for state and unknown input estimation for the active suspension system. In (Kaldas et al., 2011), a Kalman Filter algorithm is constructed for bounce velocity estimation. De Bruyne et al. (2011) present the design and development of a state estimator that accurately provides the information required by a sky-hook controller, using a minimum of sensors. In Hong and Park (2010), a road-frequency adaptive control for semi-active suspension systems is investigated. By using the data measured from a relative displacement sensor, a state estimator based on a Kalman filter for estimating the required state variables is designed. Road disturbance frequencies are estimated by using a first order zero-crossing algorithm. In Koch et al. (2010), an estimator structure for active vehicle suspension control incorporating three parallel Kalman filters has been presented.

This study introduces an integrated vehicle state estimator, comprising of a series of model based and kinematic based observers and an effectively designed merging scheme that ensures robust estimation performance even during the vehicle manoeuvres which show highly nonlinear tyre characteristics and in the existence of road inclination or bank angle. In this study, it is assumed that measurements from a 6-axis Inertial Measurement Unit (IMU) (3-axes of rotation rate measurement and 3-axes of acceleration measurement), wheel speed sensors, and steering wheel angle sensor are available. Hence, the scope of this research is to maximise the estimation performance of vehicle states with only a low-cost six-dimensional (6D) inertial measurement unit (IMU), regardless of how severely a vehicle is manoeuvred, and without the aid of a GPS.

The basic organisation of this paper is as follows: Section 2.1 contains information on the general layout of the observer with the data flow description. Section 2.2 denotes the principle behind the chassis roll angle estimator. Section 2.3 describes the method for chassis pitch angle estimation. Section 2.4 focuses on the vehicle roll (global roll) and pitch angle (global pitch) observer design. Section 2.5 describes the method to compensate the measured acceleration signals for gravity. Section 2.6 focuses on the method to estimate the vehicle longitudinal velocity. Section 2.7 describes the method to estimate the tyre vertical load. Section 2.8 presents a scheme for longitudinal/lateral tyre-force estimation. Section 2.9 describes a method for estimating the vehicle lateral and longitudinal velocity. Section 2.10 proposes an estimation procedure for the tyre slip-ratio and slip-angle, and conclusions are finally given in Section 3.

2 Observer design

2.1 General observer flow chart

The block diagram in Figure 1 explicitly shows the estimation process in its entirety.

Figure 1 Functional diagram of the estimation process (see online version for colours)

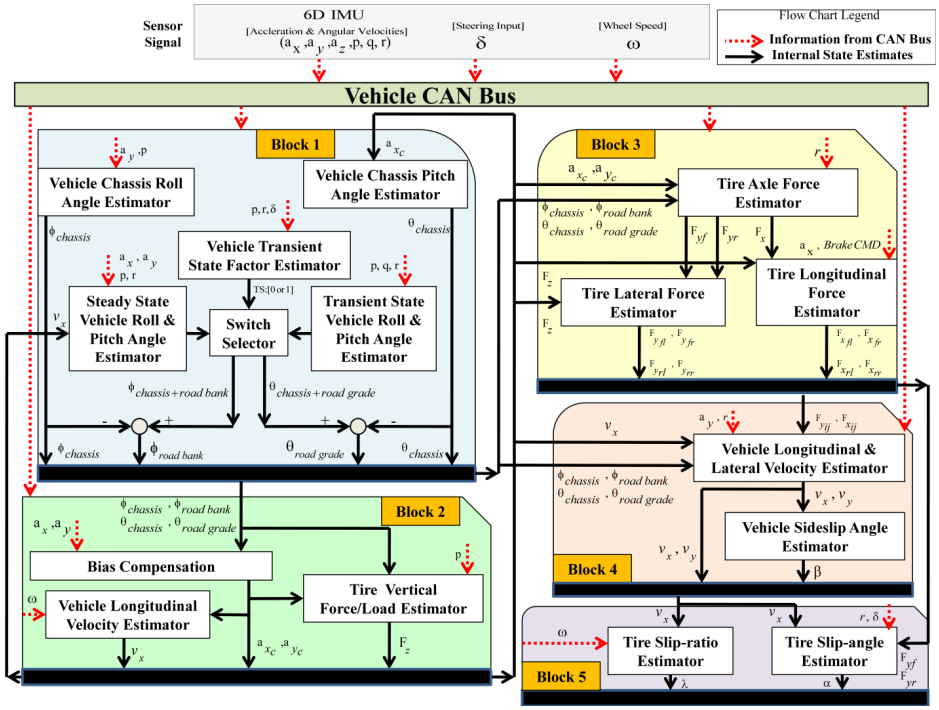

The entire process is separated into five blocks: the first block serves to identify the road bank and grade angles (using a kinematics-based observer) and vehicle chassis roll (using a Kalman filter) and pitch angles (with vehicle mass adaptation), the second block contains a bias compensation algorithm (gravity compensation in accelerometer measurements), a vehicle longitudinal speed estimation algorithm (based on the

measurements of the four wheel rotational speeds and the gravity-compensated longitudinal vehicle acceleration) and a tyre load estimation algorithm (using gravity-compensated acceleration information and roll/pitch states), the third block contains a tyre longitudinal/lateral force estimation observer (sliding-mode observer based), while the fourth block contains a nonlinear vehicle longitudinal and lateral velocity observer (based on unscented Kalman filter), designed for the purpose of vehicle side-slip estimation. Finally, the fifth block makes use of the estimations provided by the third and the fourth block to estimate the tyre slip-ratio and slip-angle (Luenberger observer based).

2.2 Vehicle chassis roll angle estimator

2.2.1 Modelling approach

Roll angle is an important variable that plays a critical role in the calculation of real-time rollover index for a vehicle (Yi et al., 2007). Vehicle models used for estimation roll angle and roll rate include:

- 3DOF model, which represents yaw, lateral and roll motions of a vehicle (Figure 2(a))
- 1DOF model, which represents only roll motion of a vehicle (Figure 2(b)).

As shown in previous work (Chen et al., 2010), roll angle estimation accuracy using the 3DOF model is adversely affected by the linear tyre model assumption. On the other hand, the 1DOF model, which does not rely on any tyre model uses the lateral acceleration directly.

Figure 2 (a) linear 3DOF yaw-roll vehicle model and (b) 1DOF roll dynamics model: (a) 3DOF vehicle model and (b) 1DOF vehicle model (see online version for colours)

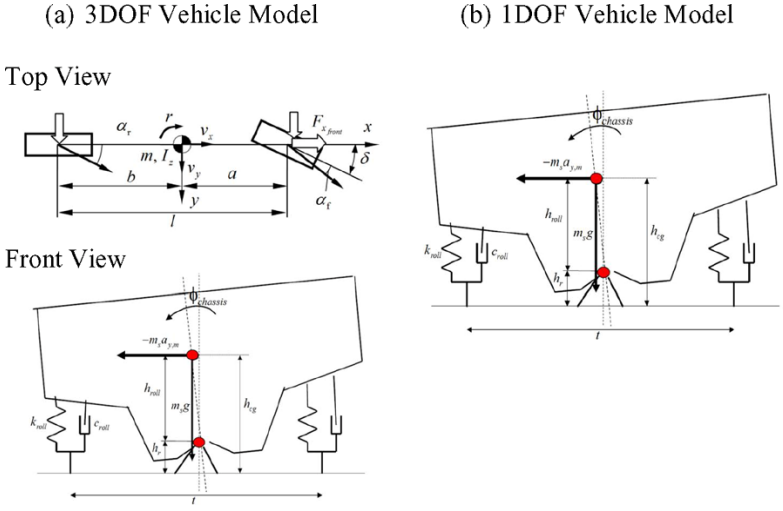

Therefore, the 1DOF model is not sensitive to the nonlinear tyre dynamics. Also, the 1DOF model has a practical advantage over the 3DOF model in terms of the required

model parameters. With these considerations, in this study, a 1DOF model was considered for designing a roll angle estimator.

Considering the effect of gravity, the equation of vehicle chassis roll motion (according to the torque balance about the roll axis) is:

$$(I_x + m_s h_{roll}^2)\ddot{\phi}_{chassis} + c_{roll}\dot{\phi}_{chassis} + k_{roll}\phi_{chassis} = -m_s h_{roll} a_{y,m} \tag{1}$$

Here $I_x + m_s h_{roll}^2$ is the moment of inertia of vehicle body with respect to the roll axis, c_{roll} is the combined roll damping of suspension and tyres, and k_{roll} is the combined roll stiffness of suspension and tyres. The lateral acceleration used in equation (1) is the measured lateral acceleration, $a_{y,m} = a_y + g\sin(\phi_{chassis})$, which includes the effect of the gravity component, contributing to the roll moment. The corresponding state-space realisation of the model described by equation (1) can be given as follows:

$$\begin{bmatrix} \dot{\phi} \\ \ddot{\phi} \end{bmatrix} = \begin{bmatrix} 0 & 1 \\ \dfrac{-k_{roll}}{I_x + m_s h_{roll}^2} & \dfrac{-c_{roll}}{I_x + m_s h_{roll}^2} \end{bmatrix} \begin{bmatrix} \phi \\ \dot{\phi} \end{bmatrix} + \begin{bmatrix} 0 \\ \dfrac{-m_s h_{roll}}{I_x + m_s h_{roll}^2} \end{bmatrix} \cdot a_{y,m} \tag{2}$$

Assuming roll rate measurement is available from a 6-axis IMU, an estimator based on the Kalman filter (Bishop, 2006) is implemented to estimate vehicle states (Figure 3). The states are roll angle and roll rate and the input is the measured lateral acceleration. The state feedback is the measured roll rate.

Figure 3 Roll estimation based on a 1DOF model (see online version for colours)

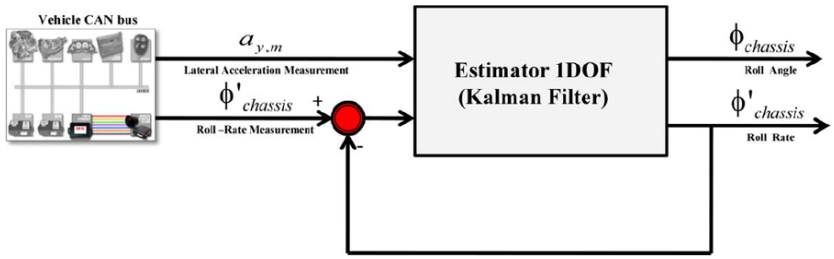

2.2.2 Estimator performance

The performance of the Kalman filter based estimator was examined under a simulated fishhook manoeuvre (Figure 4(a)) and double lane change (Figure 4(b)) to verify the effectiveness under aggressive driving conditions.

It can be concluded that even under aggressive driving conditions vehicle roll angle can accurately be estimated.

2.3 Vehicle chassis pitch angle estimator

2.3.1 Modelling approach

During a severe deceleration (acceleration) manoeuvre, the vehicle experiences a load transfer from the rear to the front (front to rear), which results in a non-zero vehicle pitch angle (Figure 5).

Figure 4 Estimator performance: (a) fishhook manoeuvre and (b) double lane change manoeuvre (see online version for colours)

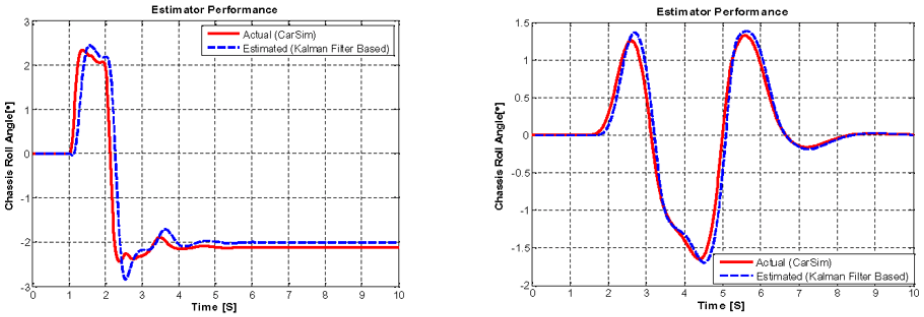

Figure 5 Longitudinal vehicular load transfer under acceleration (see online version for colours)

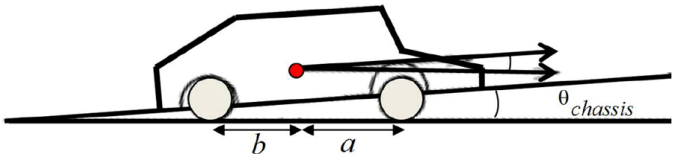

According to Hooke's law, we can compute the suspension springs compression (x) due to load variation (F_z) as $x = F_z / k_{suspension}$, where $k_{suspension}$ is the spring elastic constant. Hence, the pitch angle can be approximated by its tangent as:

$$\theta_{chassis} = \frac{2 \cdot \Delta x}{(a+b)} = \frac{2 \cdot \Delta F}{k_{suspension} \cdot (a+b)} \tag{3}$$

The longitudinal load transfer (axle load variation) can be estimated using the vehicle's longitudinal acceleration as:

$$\Delta F = \frac{m_s \cdot h_{cg}}{(a+b)} \cdot a_{x,c} \tag{4}$$

where $a_{x,c}$ is the bias-compensated longitudinal acceleration signal and is given by the expression $a_{x,c} = a_{x,m} + \text{gsin}(_{chassis})$. A methodology to compensate the measured acceleration signal for the gravity component is given in Section 2.5. Substituting equation (4) in equation (3), we get an expression for the chassis pitch angle as:

$$\theta_{chassis} = \frac{2 \cdot m_s \cdot h_{cg}}{k_{suspension} \cdot (a+b)^2} \cdot a_{x,c} \tag{5}$$

Since chassis pitch angle is calculated through a linear model, the parameters used in the model are functions of characteristics such as the height of the CoG and the sprung mass. One challenge with using these parameters in computing $\theta_{chassis}$ is that they vary with the vehicle loading conditions. If the above parameters are fixed at certain nominal values, it is conceivable that optimal estimation performance may not be achieved under a different

loading condition. To improve the overall performance of the estimation process, it is desirable to estimate and update the vehicle parameters periodically or adaptively adjust them in real time based on the actual behaviour of the vehicle.

2.3.2 Vehicle sprung mass estimation

The estimation approach proposed here is a model-based approach, i.e., using equations for the longitudinal motion of the vehicle (Figure 6(a)). Vehicle acceleration is a result of a combination of wheel drive and braking torques and the road loads on the vehicle. The dynamic equation for the vehicle motion is:

$$m\dot{v}_x = \sum F_x - F_{aero\ drag} - F_{grade} - F_{rolling\ resistance} \tag{6}$$

where:

$\sum F_x$: Summation of the tyre forces generated at all the four tyres

$F_{aero\ drag}$: Aerodynamic drag force $\left(\frac{1}{2}\rho C_d A_f v_x^2\right)$

F_{grade} : Road grade force ($mgsin\theta_{grade}$)

$F_{rolling\ resistance}$: Rolling resistance ($f_r mgcos\theta_{grade}$)

$$or\ m\dot{v}_x = \left(F_{x_{fl}} + F_{x_{fr}} + F_{x_{rl}} + F_{x_{rr}}\right) - \frac{1}{2}\rho C_d A_f v_x^2 - mgsin\theta_{grade} - f_r mgcos\theta_{grade}$$

Figure 6 (a) Longitudinal vehicle dynamics model and (b) simplified wheel dynamics model (see online version for colours)

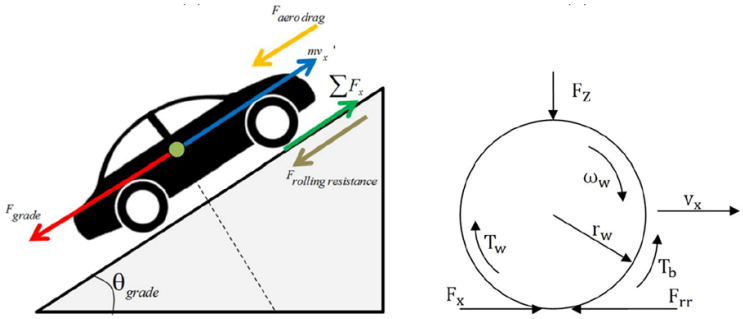

Rearranging the above Equation yields an expression for the vehicle mass as:

$$m = \frac{\left(F_{x_{fl}} + F_{x_{fr}} + F_{x_{rl}} + F_{x_{rr}}\right) - \frac{1}{2}\rho C_d A_f v_x^2}{\dot{v}_x + g\sin\theta_{grade} + f_r g\cos\theta_{grade}} \tag{7}$$

From the above expression, we can see that an estimate of the vehicle mass can be made by using information about the longitudinal tyre forces, vehicle longitudinal velocity and

road grade. To achieve the objective of estimating vehicle mass, an integrated estimation scheme is proposed. The estimation scheme consists of three key estimator blocks;

- tyre longitudinal force estimator
- vehicle longitudinal velocity estimator;
- road bank-grade angle estimator.

The tyre longitudinal force estimator is based on a simplified wheel dynamics model (Figure 6(b)). The dynamic equation for the angular motion of the wheel is given as:

$$J\dot{\omega}_w = (T_w - T_b) - F_x r_w - F_{rr} r_w \tag{8}$$

where the subscripts have been omitted for convenience. The same estimator and equations hold true for all the wheels. Rearranging equation (8) yields an expression for the longitudinal force as:

$$F_x = \frac{(T_w - T_b) - J\dot{\omega}_w}{r_w} - F_{rr} \tag{9}$$

Here the wheel drive torque (T_w) can be estimated by using the turbine torque, the turbine angular velocity, and the wheel angular velocity (Masmoudi and Hedrick, 1992). It is assumed that the brake pressure of each wheel is an available signal. Therefore, the brake torque (T_b) can be computed by the brake gain (k_{bf}, k_{br}). F_{rr}, the wheel rolling resistance force is given by the expression:

$$F_{rr} = 0.005 + 3.24 \cdot 0.01 \cdot (r_w \cdot \omega_w)^2 \tag{10}$$

In a previous work (Hoseinnezhad and Bab-Hadiashar, 2011), it has been shown that the accuracy of longitudinal force estimation using equation (8) heavily depends on the accuracy of the tyre effective rolling radius (r_w), and therefore, obtaining an accurate estimate of r_w is crucial. The tyre effective rolling radius (r_w) can be determined by the vertical load (estimation methodology for the vertical load is explained in Section 2.7) as:

$$r_{w,i} = r_o - \frac{F_{z,i}}{k_t} \tag{11}$$

Even though equation (9) presents a relatively simple method to estimate the longitudinal tyre force (i.e., we can calculate the longitudinal tyre force directly using equation (9), or use a recursive least squares (RLS) method for a smoother estimation), it is not advisable to use this approach, since in real-world conditions finding the time derivative of angular wheel speed signals ($\dot{\omega}_w$) can pose some challenges. To avoid the need to take derivatives of ω_w, a sliding mode observer (SMO) based estimation scheme is used (Rajamani et al., 2012). The SMO uses a sliding mode structure, with the state estimate

($\dot{\omega}_w$) evolving according to the wheel dynamics model, the force model $\dot{F}_x = 0$, i.e., tyre forces are modelled with a random walk model and the sign of the measurement estimation error (difference between actual (ω_w) and estimated ($\dot{\omega}_w$) angular wheel speed) as:

$$J\dot{\hat{\omega}}_w = (T_w - T_b) - \hat{F}_x r_w - F_{rr} r_w + k_1 sgn(\omega_w - \hat{\omega}_w) \tag{12}$$

$$\dot{\hat{F}}_x = k_2 sgn(\omega_w - \hat{\omega}_w) \tag{13}$$

Here k_1 & k_2 are the observer gains and *sgn* denotes signum function defined as:

$$\text{sgn}(s(t)) = \begin{cases} 1, & \text{if } s(t) > 0 \\ 0, & \text{if } s(t) = 0 \\ -1, & \text{if } s(t) < 0 \end{cases} \tag{14}$$

It is known that the discontinuous switching functions can be approximated by their continuous switching functions to avoid the chattering of the control force and to achieve the exponential stability. Instead of signum function, a saturation function has been used via introducing a thin boundary layer around the sliding surface to avoid chattering. For a smoother change of the switching signal, a hyperbolic tangent function has also been used to improve the switching control effort. The results (Figure 7(a)–(b)) show that the estimated longitudinal forces match the simulated forces very well. The proposed observer based on equations (13) and (14) thus ensures stable estimation of the longitudinal tyre force. As previously mentioned, apart from the longitudinal tyre force, the other variables required to estimate the vehicle mass include: road grade angle and vehicle longitudinal velocity. The road grade angle (θ_{grade}) can be determined using a kinematics-based observer, as explained in Section 2.5. The vehicle longitudinal velocity (v_x) can be determined using the measurement of the four-wheel rotational speed and longitudinal vehicle acceleration, as explained in Section 2.6. Finally, using information from the three estimators, vehicle mass can be estimated using equation (7). Even though we can directly use equation (7), using a Recursive Least Squares (RLS) algorithm (by rewriting equation (7) into a standard parameter identification form) results in smoother estimates of the vehicle mass, as shown in Figure 8.

2.3.3 Estimator performance

The performance of the chassis pitch angle estimator (refer equation (5), with vehicle mass adaptation) was evaluated for a high speed straight-line braking manoeuvre (100-0 Kph) for constant friction coefficient ($\mu_{constant}$) (Figure 9(a)), and varying friction coefficient ($\mu_{varying}$) (Figure 9(b)) conditions. Satisfactory results were obtained in both cases, as shown in Figure 9.

Figure 7 Longitudinal force (individual tyre) estimator performance: a) high μ surface condition and (b) low μ surface condition (see online version for colours)

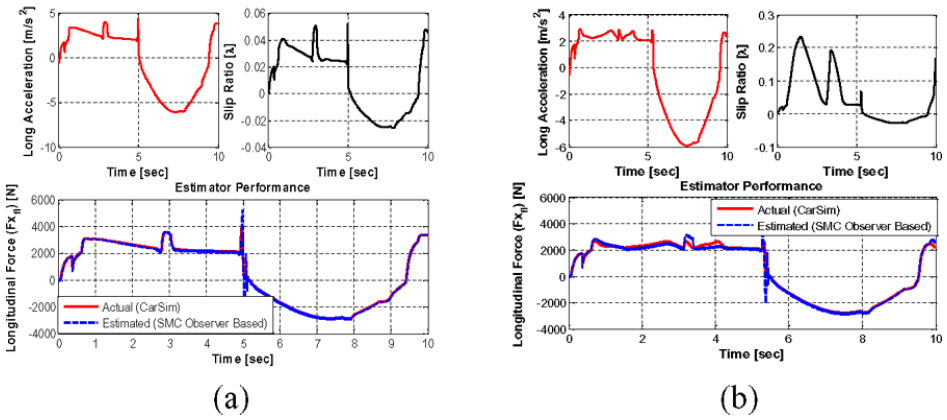

Figure 8 Vehicle mass estimation results: (a) D-class vehicle (sedan) driving on low μ surface and (b) B-class vehicle (hatchback) driving on high μ surface (see online version for colours)

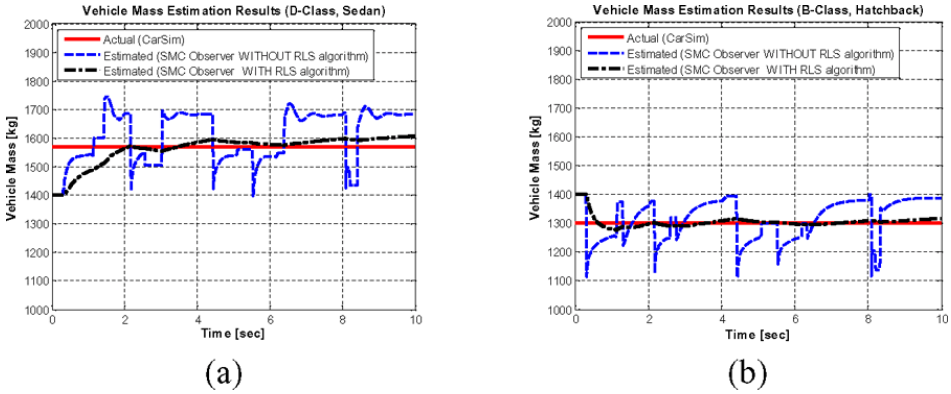

Figure 9 Estimator performance: (a) straight-line braking manoeuvre (constant μ condition) and (b) straight-line braking manoeuvre (varying μ condition) (see online version for colours)

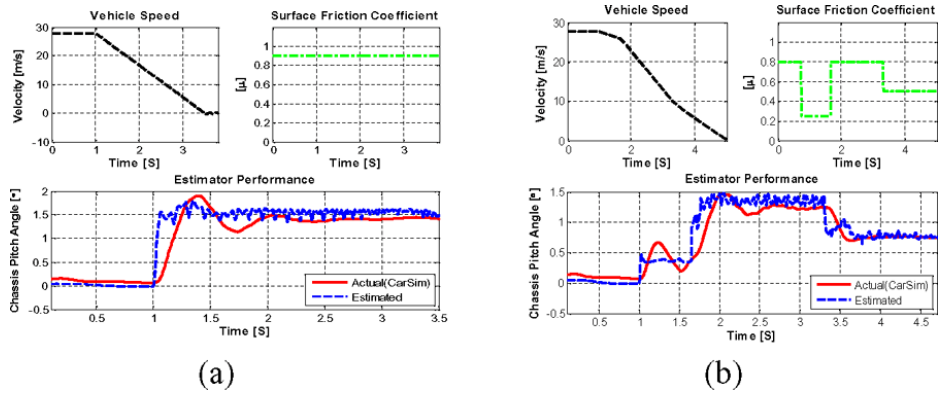

2.4 Vehicle roll and pitch angle estimator

Knowledge of the vehicle roll and pitch angle is very important for satisfactory control performance. Analysis presented in Sections 2.2 and 2.3 described a methodology to estimate the vehicle chassis roll (local roll) and chassis pitch (local pitch) angle. The vehicle roll angle (global roll) consists of a combination of vehicle chassis roll angle and road bank angle:

$$\phi_{vehicle\ roll} = \phi_{chassis} + \phi_{road\ bank} \tag{15}$$

Similarly, the vehicle pitch angle consists of the combination of vehicle chassis pitch angle and road grade angle:

$$\theta_{vehicle\ pitch} = \theta_{chassis} + \theta_{road\ grade} \tag{16}$$

The effect of vehicle chassis roll and pitch, as well as the dynamically changing road bank and road grade is significant because they directly lead to the gravity components measured by the accelerometers, as shown below:

$$\begin{aligned} a_{x,m} &= a_x - g \cdot \sin(\theta_{vehicle\ pitch}) \\ \Rightarrow a_{x,m} &= (\dot{v}_x - r \cdot v_y) - (g \cdot \sin(\theta_{vehicle\ pitch})) \end{aligned} \tag{17}$$

$$\begin{aligned} a_{y,m} &= a_y + g \cdot \sin\left(\phi_{vehicle\,roll}\right) \\ &\quad \cos(\theta_{vehicle\ pitch}) \\ \Rightarrow a_{y,m} &= (\dot{v}_y + r \cdot v_x) + (g \cdot \sin\left(\phi_{vehicle\,roll}\right)) \\ &\quad \cdot \cos(\theta_{vehicle\ pitch}) \quad) \end{aligned} \tag{18}$$

Rearranging the above equations, we have expressions for the vehicle chassis roll and pitch angles as:

$$\begin{aligned} \theta_{vehicle\ pitch} &= arcsin\left(\frac{\dot{v}_x - r \cdot v_y - a_{x,m}}{g}\right) \\ \phi_{vehicle\ roll} &= arcsin\left(\frac{a_{y,m} - \dot{v}_y - r \cdot v_x}{g \cdot \cos(\theta_{vehicle\ pitch})}\right) \end{aligned} \tag{19}$$

In the following section, a methodology to estimate the vehicle roll and pitch angles under steady state conditions is presented.

2.4.1 Steady state vehicle roll and pitch angle estimator

In this section, steady state estimates of the vehicle pitch and roll angles are presented by utilising the sensors typically available on vehicles equipped with electronic stability program (ESP) or yaw dynamics control (YDC). As seen from equation (19), vehicle pitch and roll angles can be calculated if $v_x, v_y, \dot{v}_x$ and $\dot{v}_y$ are available. Although it is possible to obtain fairly accurate v_x and thus $\dot{v}_x$ from wheel speed sensors when the

wheel slip is small (see Section 2.6 for details), v_y and v_y are generally not available on current production vehicles. Thus equation (19) cannot be implemented. Fortunately, during many manoeuvres, v_y or v_y is relatively small and can be neglected. In such cases, the so-called steady state pitch and roll angles, $\theta_{vehicle\ pitch_{SS}}$ and $\phi_{vehicle\ roll_{SS}}$, respectively, are given by the following equations:

$$\theta_{vehicle\ pitch_{SS}} = arcsin\left(\frac{v_x^{\cdot} - a_{x,m}}{g}\right)$$
$$\phi_{vehicle\ roll_{SS}} = arcsin\left(\frac{a_{y,m} - r \cdot v_x}{g \cdot \cos(\theta_{vehicle\ pitch_{SS}})}\right) \tag{20}$$

The steady state estimates obtained from the algebraic manipulation of the kinematic relationships only captures the low-frequency component of the vehicle attitude (Figure 10)

Figure 10 Performance of the steady state vehicle roll angle estimator: (a) constant speed straight-line driving (steady state) on a banked road and (b) double lane change manoeuvre (transient state) on a banked road (see online version for colours)

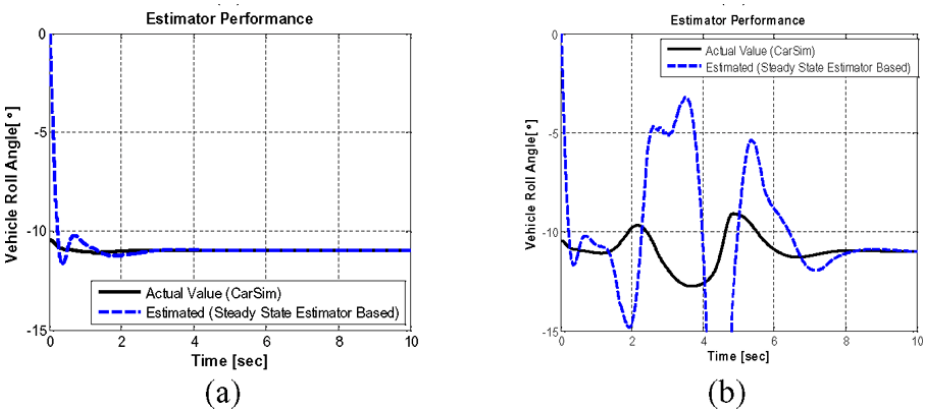

The underlying reason for the poor performance of the steady state estimator (Figure 10(b)) is the assumption ($v_y \approx 0$ or $v_y^{\cdot} \approx 0$) on which the estimator works. This assumption is often violated during real life driving situations. For example, a vehicle performing an object avoidance manoeuvre on a highway ramp or a vehicle negotiating a mountain road may experience significant bank angle variations during the transient manoeuvre. Hence this estimate would contain significant bias in transient manoeuvres. In the following section, a methodology to estimate the vehicle roll and pitch angles under transient state conditions is presented.

2.4.2 Transient state vehicle roll and pitch angle estimator

Without loss of generality, it is assumed that the IMU is placed at the vehicle center of gravity, and there is no misalignment with respect to the vehicle body frame. Using the

kinematic relationship between IMU output (vehicle-fixed frame) and the derivatives of the Euler angles (inertial frame), and assuming that the rotation rate of the earth is negligible, the equations of vehicle motion can be written as (Greenwood, 1988):

$$\begin{aligned}\dot{\phi}_{vehicle\,roll} &= p + \left(q \cdot \sin\phi_{vehicle\,roll} + r \cdot \cos\phi_{vehicle\,roll}\right) \\ &\quad \cdot tan(\theta_{vehicle\,pitch}) \\ \dot{\theta}_{vehicle\,pitch} &= q \cdot \cos\phi_{vehicle\,roll} - r \cdot \sin\phi_{vehicle\,roll} \\ \dot{\psi}_{vehicle\,yaw} &= \left(q \cdot \sin\phi_{vehicle\,roll} + r \cdot \cos\phi_{vehicle\,roll}\right) \\ &\quad \cdot \sec(\theta_{vehicle\,pitch})\end{aligned} \tag{21}$$

From the above relationships we can see that, theoretically, the vehicle roll ($\phi_{vehicle\ pitch}$) and pitch angles ($\theta_{vehicle\,pitch}$) can be computed via mathematical integration (open-loop integration), if the initial condition is known and angular rates (p,q,r) are measured by the gyro sensors. In practice, however, direct integration tends to drift due to sensor bias and inevitable numerical errors. To overcome limitations of an open-loop integration process, an alternative method is proposed. With the addition of an observer feedback term, $k(\theta_{chassis} - \hat{\theta}_{chassis})$, a new closed-loop observer is designed, motivated by (K. Cho et al., 2010), to estimate the vehicle roll-pitch angle under transient state conditions as:

$$\begin{aligned}\dot{\phi}_{vehicle\,roll_{TS}} &= p + \left(q \cdot \sin\phi_{vehicle\,roll_{TS}} + r \cdot \cos\phi_{vehicle\,roll_{TS}}\right) \\ &\quad \cdot tan(\theta_{vehicle\,pitch_{TS}}) \\ &\quad + k(\theta_{chassis} - \hat{\theta}_{chassis}) \\ \dot{\theta}_{vehicle\,pitch_{TS}} &= q \cdot \cos\phi_{vehicle\,roll_{TS}} - r \cdot \sin\phi_{vehicle\,roll_{TS}}\end{aligned} \tag{22}$$

Where the subscript TS denotes transient state. The observer feedback term ($k(\theta_{chassis} - \hat{\theta}_{chassis})$), basically consists of a measurement estimation error, i.e., difference between actual $\theta_{chassis}$ and estimated $\hat{\theta}_{chassis}$ chassis roll angles. Here $\theta_{chassis}$ is obtained using a 1DOF roll dynamics model in conjunction with a Kalman filter (details given in Section 2.2). $\hat{\theta}_{chassis}$, is obtained using information about the lateral load transfer ratio (LTR), where the LTR is estimated using dynamic tyre load estimates (details given in Section 2.7). To fuse the steady state and transient state estimates, an index known as the vehicle transient state factor (VTSF) is defined, which represents the state of the vehicle (i.e., VTSF = 1 (Transient State); VTSF = 0 (Steady State)).

The vehicle transient state factor (VTSF) is characterised as a function of the vehicle roll rate, derivative of the steering wheel angle and yaw rate. Finally, the vehicle roll angle is estimated using the vehicle steady state and transient state roll angles based on the vehicle state index switching (Figure 11) as:

$$\phi_{vehicle\,roll} = \left[VTSF * \int \left(\begin{array}{c} p + \left(q \cdot \sin \phi_{vehicle\,roll_{TS}} + r \cdot \cos \phi_{vehicle\,roll_{TS}} \right) \\ \cdot \tan \left(\theta_{vehicle\,pitch_{TS}} \right) \\ + k \left(\theta_{chassis} - \hat{}_{chassis} \right) \\ + \left(\phi^{*}_{vehicle\,roll_{SS}} \right) \end{array} \right) \right] + \left[(1 - VTSF) \cdot \phi_{vehicle\,roll_{SS}} \right] \tag{23}$$

Where $\phi^{*}_{vehicle\,roll_{SS}}$ is the vehicle steady state roll angle when the state index switches from 1 to 0. It is used as an initial condition for the vehicle transient roll angle estimator.

An updated estimate of the vehicle pitch angle is derived using the following expression:

$$\dot{\theta}_{vehicle\,pitch} = q \cdot \cos \phi_{vehicle\,roll} - r \cdot \sin \phi_{vehicle\,roll} \tag{24}$$

Figure 11 Schematic diagram of the proposed vehicle roll/pitch angle estimation process (see online version for colours)

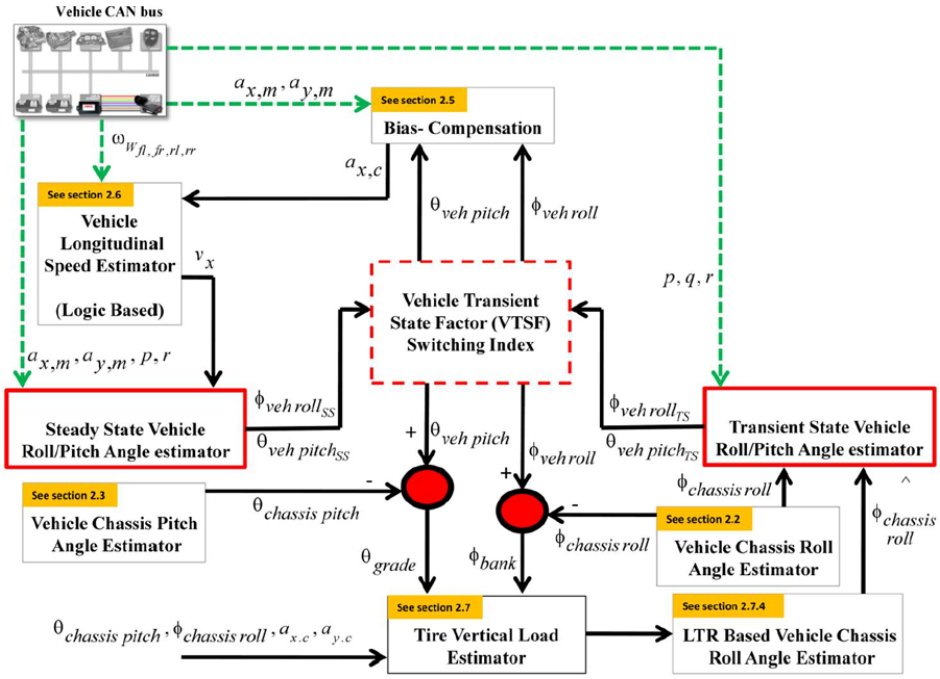

2.4.3 Estimator performance

The performance of the designed roll/pitch angle estimator was evaluated for a range of different simulations cases (Table 2).

Table 2 Simulation cases

	Vehicle speed (Kph)	*Friction coefficient (μ)*	*Test manoeuvre*	*Road bank angle (°)*	*Road grade angle (°)*
Case 1	140	0.85	Double lane change	0°	0°
Case 2	140	0.85	Double lane change	0°-18°- 0°	0°

Figure 12 shows that the proposed observer can estimate the vehicle states (roll/pitch angle) successfully even for challenging (aggressive manoeuvring) operating conditions.

Figure 12 Vehicle roll/pitch angle estimator performance (ref Table 2 for a description of the simulation conditions) (see online version for colours)

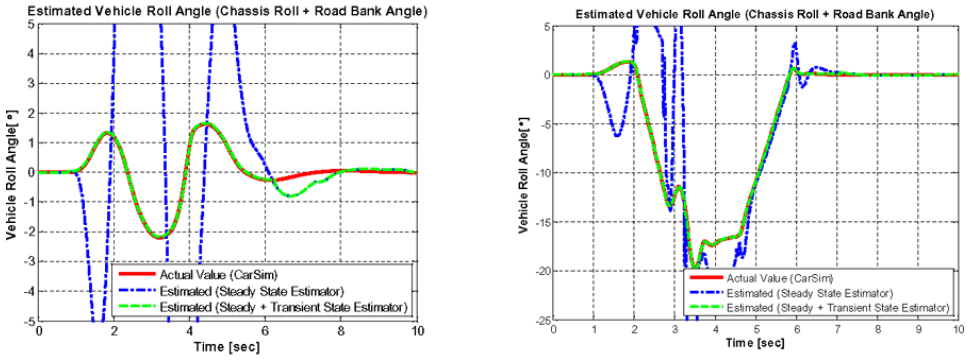

2.5 Bias Compensation

The measured lateral/longitudinal acceleration has both lateral/longitudinal dynamics components and gravity components due to road bank/grade and chassis angles. Using the real-time vehicle roll and pitch angle estimates (as described in Section 2.4), the measured acceleration signals are compensated for the gravity components using:

$$a_{x,c} = a_{x,m} + g \cdot \sin(\theta_{vehicle\ pitch}) \tag{25}$$

$$a_{y,c} = a_{y,m} - g \cdot \sin(\phi_{vehicle\ roll}) \cdot \cos(\theta_{vehicle\ pitch}) \tag{26}$$

Vehicle sideslip angle is estimated using a simple integration method to verify whether the compensation of the lateral acceleration is useful to estimate the side-slip angle. The integration method to estimate the side-slip angle is as follows:

$$\beta = \frac{v_y}{v_x} = \int \frac{a_{y,m} - (g \cdot \sin(\phi_{vehicle\ roll}) \cdot \cos(\theta_{vehicle\ pitch}) \ ) - r \cdot v_x}{v_x} \mathrm{d}t \tag{27}$$

$$or\ \beta = \frac{v_y}{v_x} = \int \frac{a_{y,c} - r \cdot v_x}{v_x} \mathrm{d}t \tag{28}$$

The simulation results show (Figure 13) that the compensated lateral acceleration can be used directly to estimate the vehicle side-slip angle.

Figure 13 Vehicle sideslip angle estimation using a simple integration method: (a) double lane change steering/high mu(0.85/120 kph/bank(0 – 18- 0 deg) and (b) fishhook steering/high mu (0.85/80kph/flat surface) (see online version for colours)

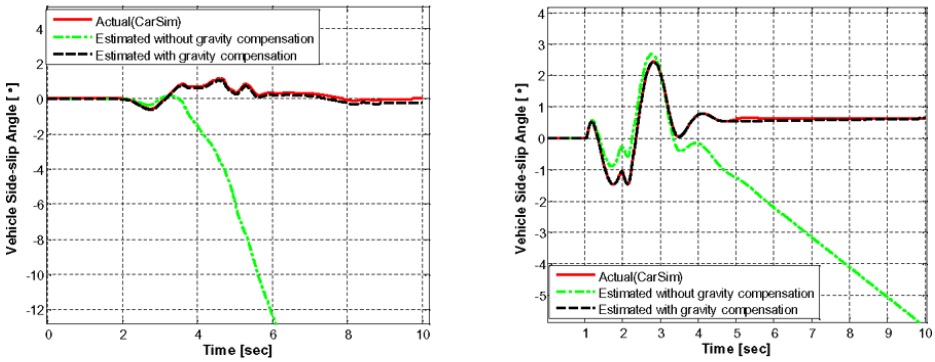

2.6 *Vehicle longitudinal velocity estimator*

2.6.1 *Estimation methodology*

An integrated state estimation scheme (refer Figure 1) requires reliable vehicle speed information. It is much harder to estimate the vehicle speed during braking than in traction, since in the former case all four wheels are slipping. The proposed vehicle speed estimation algorithm (Figure 14) is based on the measurement of the four-wheel rotational speed and longitudinal vehicle acceleration.

Figure 14 Estimation algorithm data flow chart

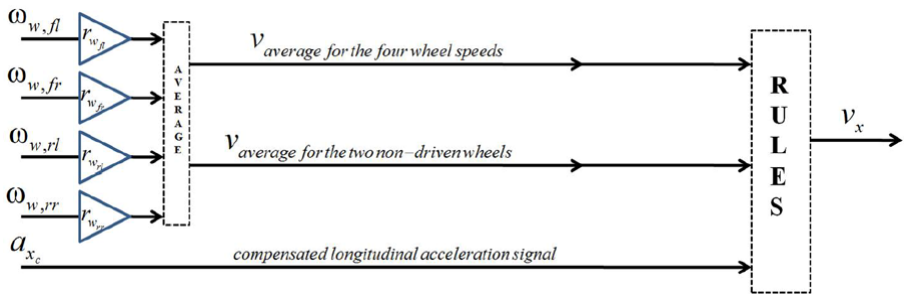

The estimator uses a structure based on the work of reference (Tanelli et al., 2006). The main advantage of this approach is the low computation burden, as compared to some of the previous work proposed in literature (Jiang and Gao, 2000; Watanabe et al., 1992; Klein et al., 1996; Kobayashi et al., 1995), which suffer from high computational complexity. The longitudinal acceleration signal is supposed to have been properly corrected according to the discussion given in Section 2.5 as:

$$a_{x,c} = a_{x,m} + g \cdot \sin(\theta_{vehicle\ pitch}) \tag{29}$$

The effective tyre radius (r_w) required to estimate the linear wheel speed can be determined using the tyre vertical load information (load estimation methodology described in Section 2.7) as:

$$r_{w,i} = r - \frac{F_{z,i}}{k_t} \tag{30}$$

At each sampling instant, the following auxiliary signals are computed:

$v_{average}$: average of the four wheel speeds

$v_{non-driven\ average}$: averageofthe two non – driven wheel speeds.

The estimation algorithm behaviour changes according to the status of the vehicle, which is represented by the following four states:

State 1: Low Speed

State 2: Accelerating

State 3: Constant speed or is softly braking

State 4: Braking.

The status of the vehicle is determined using the following threshold values:

v_{min} : vehile speed threshold

a_{acc} : vehicle acceleration threshold

a_{dcc} : vehicle decceleration threshold

When the vehicle has very low or constant speed, the estimated vehicle speed is obtained as the average of the four-wheel speeds. When the car is accelerating, instead, as the driving wheels have a non–null longitudinal slip due to traction force, the estimated vehicle speed is obtained as the average of the non–driving wheels. During an extreme braking manoeuvre, the estimated vehicle speed is obtained via an open-loop integration of the corrected accelerometer signal, augmented with a backward integration phase to cope with initialisation errors (Table 3).

Table 3 Estimation algorithm rules

Rule chart: Vehicle status and velocity estimation			
Case 1	*Case 2*	*Case 3*	*Case 4*
$if\ v_{average} < v_{min}$	$if\ v_{average} > v_{min}$ & $a_x > a_{acc}$	$if\ v_{average} > v_{min}$ & $a_{dcc} < a_x < a_{acc}$	$if\ v_{average} > v_{min}$ & $a_x < a_{dcc}$
Vehicle status: Low speed	Vehicle status: Acceleration	Vehicle status: Constant speed or softly braking	Vehicle status: Braking speed is estimated using a recursive rule
$v_x = v_{average}$	$v_x = v_{nondriven\ avg}$	$v_x = v_{average}$	$v_t = v_{t-1} + a_t * dt$
Thresholds: $v_{min} = 2\frac{m}{s}$; $a_{acc} = 0.1\frac{m}{s^2}$; $a_{dcc} = -0.8\frac{m}{s^2}$			

2.6.2 Estimator performance

The performance of the velocity estimator was evaluated for an aggressive straight-line braking manoeuvre (Figure 15).

According to these encouraging results (Figure 15(a)), the output of the longitudinal vehicle speed estimation algorithm could also be employed for reliably computing the longitudinal wheel slip (Figure 15(b)).

Figure 15 (a) Estimated vehicle speed compared with the reference vehicle speed and (b) estimated wheel slip (top) and absolute error (bottom) compared with the reference wheel slip (see online version for colours)

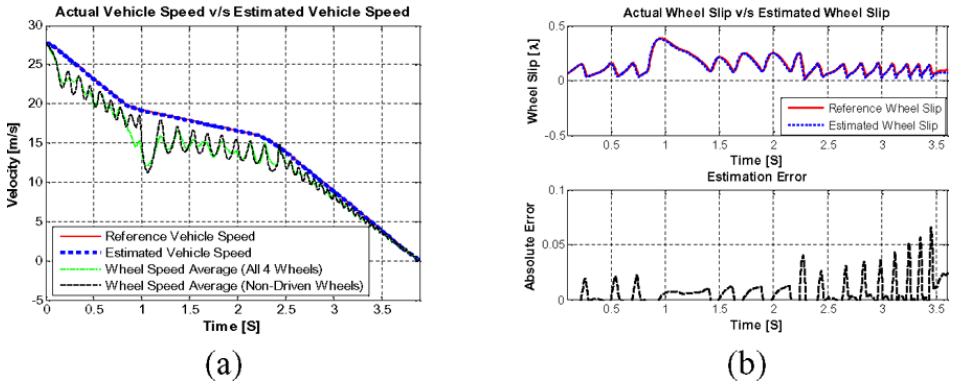

2.7 Tyre vertical load estimator

The vertical tyre forces can be estimated by the summation of longitudinal load transfer, lateral load transfer and the static normal force. The estimates of the vertical tyre forces can be represented as follows:

$$\begin{aligned} Fz_{fl} &= \frac{Fz_{front\ axle}}{2} - W_{Lateral\ Load\ Transfer} - W_{Longitudinal\ Load\ Transfer} \\ Fz_{fr} &= \frac{Fz_{front\ axle}}{2} + W_{Lateral\ Load\ Transfer} - W_{Longitudinal\ Load\ Transfer} \\ Fz_{rl} &= \frac{Fz_{rear\ axle}}{2} - W_{Lateral\ Load\ Transfer} + W_{Longitudinal\ Load\ Transfer} \\ Fz_{rr} &= \frac{Fz_{rear\ axle}}{2} + W_{Lateral\ Load\ Transfer} + W_{Longitudinal\ Load\ Transfer} \end{aligned} \tag{31}$$

Where the axle load distribution is strictly a function of the vehicle geometry and is given as:

$$\begin{aligned} Fz_{front\ axle} &= mg \cdot \frac{b}{a+b} \\ Fz_{rear\ axle} &= mg \cdot \frac{a}{a+b} \end{aligned} \tag{32}$$

The vehicle mass (m) can be estimated adaptively using an estimation scheme described in Section 2.3.2. The lateral and longitudinal load transfer terms can be estimated using the vehicle's roll model (Figure 2(a)) and longitudinal models (Figure 6(a)) as:

$$W_{Lateral\ Load\ Transfer} = \frac{\left(\frac{\left(m_s \cdot h_r + m_u \cdot h_a\right)}{t} \cdot a_{y,c}\right) + \left(\frac{k_{roll} \cdot \phi_{chassis} + c_{roll} \cdot \dot{\phi}_{chassis}}{t}\right)}{2}$$
$$W_{Longitudinal\ Load\ Transfer} = \frac{m_s \cdot h_{cg}}{2(a+b)} \cdot a_{x,c} \tag{33}$$

The roll sates required to estimate the lateral load transfer term can be obtained using a vehicle roll state estimator, as described in Section 2.4.

2.7.1 Effect of grade angle on the load distribution

In this case, the lower tyres (rear tyres, going up and front tyres, going down) become more heavily loaded. Load distribution can be determined by summing the moments around the tyre-road contact points, leading to equations:

$$Fz_{front\ axle} = mg \cdot \frac{b}{a+b} \cdot \cos\theta_{road\ grade} - mg \cdot \frac{h_{cg}}{a+b} \cdot \sin\theta_{road\ grade}$$
$$Fz_{rear\ axle} = mg \cdot \frac{a}{a+b} \cdot \cos\theta_{road\ grade} + mg \cdot \frac{h_{cg}}{a+b} \cdot \sin\theta_{road\ grade} \tag{34}$$

2.7.2 Effect of bank angle on the load distribution

A bank causes the load on the interior (lower) tries to increase, while the load on the exterior (upper) tyres decreases. The formulas for the change in loads on the tyre are:

$$Fz_{fl} = \frac{Fz_{front\ axle}}{2} \cdot \cos\phi_{vehicle\ roll} - \frac{Fz_{front\ axle} \cdot h_{cg}}{t} \cdot \sin\phi_{vehicle\ roll}$$
$$Fz_{fr} = \frac{Fz_{front\ axle}}{2} \cdot \cos\phi_{vehicle\ roll} + \frac{Fz_{front\ axle} \cdot h_{cg}}{t} \cdot \sin\phi_{vehicle\ roll}$$
$$Fz_{rl} = \frac{Fz_{rear\ axle}}{2} \cdot \cos\phi_{vehicle\ roll} - \frac{Fz_{rear\ axle} \cdot h_{cg}}{t} \cdot \sin\phi_{vehicle\ roll}$$
$$Fz_{rr} = \frac{Fz_{rear\ axle}}{2} \cdot \cos\phi_{vehicle\ roll} + \frac{Fz_{rear\ axle} \cdot h_{cg}}{t} \cdot v\phi_{vehicle\ roll} \tag{35}$$

2.7.3 Estimator performance

To investigate the performance of the proposed vertical load estimator, simulations have been conducted for wide range of driving manoeuvres (Table 4), without including any road disturbances.

Table 4 Simulation cases

	Vehicle Speed (Kph)	*Friction Coefficient (μ)*	*Test manoeuvre*	*Road Bank Angle (°)*	*Road Grade Angle (°)*
Case 1	140	Varying (high-low-high)	Double lane change	0°	0°
Case 2	80	0.85	Fishhook	3°	3°

The comparison of the estimated vertical forces using the algorithm described in Section 2.7 and actual forces using the CarSim software is presented in Figures 16 and 17. Results show that the estimated vertical forces match the simulated forces well.

Figure 16 Test condition: double lane change manoeuvre (varying μ condition) (see online version for colours)

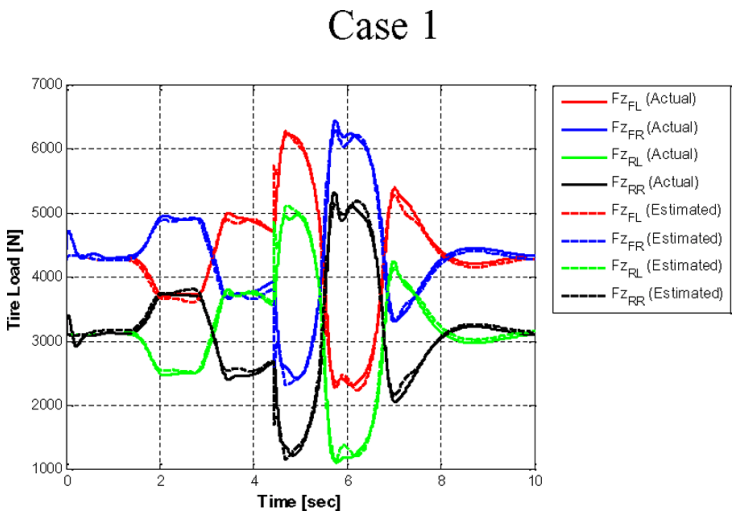

Figure 17 Test condition: fishhook manoeuvre (constant μ, banked (3°) and graded road (2°) condition) (see online version for colours)

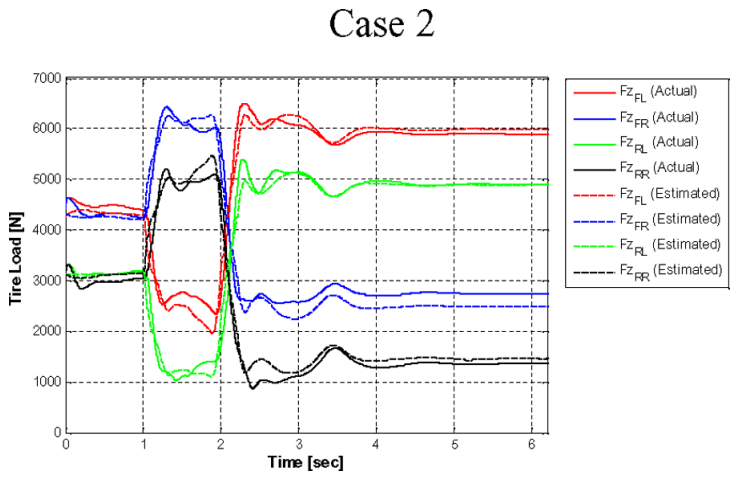

2.8 Tyre longitudinal and lateral force estimator

2.8.1 Longitudinal force estimator

In the case of a normal driving situation, longitudinal force estimators designed at the previous time instant (i.e., wheel dynamics based observer) show good performance. However, during extreme manoeuvring conditions, where the slip-ratio is large, the performance of the estimator is not satisfactory, since the longitudinal tyre-force estimator based on wheel dynamics model does not take into consideration the effects of deformation slip or wheel slip. To overcome this drawback (unsatisfactory performance under high-slip conditions) of a wheel dynamic based observer, a tyre model based closed-loop feedback observer is proposed. It is possible to use the commonly used tyre models such as the Magic Formula (MF for short) tyre model for accurate modelling, but this would result in heavy computation work which is usually beyond the computation authority of the on-board microprocessors. The estimator concept used here relies on a physically derived tyre model called the Dugoff tyre model. In its simplest formulation, the model describes the relationship between the tyre force and the slip as a function of two parameters, the tyre stiffness ($C_{x,y}$) and the tyre to road friction coefficient (μ). The tyre stiffness describes the inclination of the force-slip relation at small slips whereas the friction coefficient describes its curvature and peak value.

Dugoff-tyre model can be expressed as follows:

$$F_x = C_x \cdot \frac{s}{1+s} \cdot f(\lambda) \tag{36}$$

$$F_y = C \cdot \frac{\tan(\alpha)}{1+s} . f(\lambda) \tag{37}$$

where λ is related to tyre-road friction coefficient (μ); λ and function $f(\lambda)$ are defined, as follows:

$$\lambda = \frac{\mu \cdot F_z \cdot (1+s)}{2\sqrt{(C_x s)^2 + (C_y \tan\alpha)^2}} \tag{38}$$

$$f(\lambda) = \begin{cases} (2-\lambda)\lambda, \lambda < 1 \\ 1, \lambda \geq 1 \end{cases} \tag{39}$$

Under pure longitudinal slip conditions, the above equations simplify to:

$$F_x = C_x \cdot \frac{s}{1+s} \cdot f(\lambda) \tag{40}$$

$$f(\lambda) = \begin{cases} (2-\lambda)\lambda, & \text{if } \lambda < 1 \\ 1, & \text{otherwise} \end{cases} \tag{41}$$

$$\lambda = \frac{\mu_x \cdot F_z \cdot (1+s)}{2C_x \mid s \mid} \tag{42}$$

$$s = \frac{\omega \cdot r_w - v_x}{\max(\omega \cdot r_w, v_x)} \tag{43}$$

Figure 18(a) shows the comparison between the longitudinal forces calculated by the Dugoff and MF tyre models. This comparison shows that there is no peak point in the Dugoff model, and the peak value is much smaller than the MF model. Also, the difference in the two models is larger when the slip-ratio is high (i.e., a larger difference in the unstable/saturation region can be seen). Previous publications (Ding and Taheri, 2010) have shown that the above stated discrepancies between Dugoff-tyre and MF-tyre models can be reduced if different tyre/road friction coefficients are taken for different magnitudes of slip-ratio.

Figure 18 (a) tyre forces calculated by the dugoff and MF model and (b) tyre forces calculated by the modified dugoff and MF model (see online version for colours)

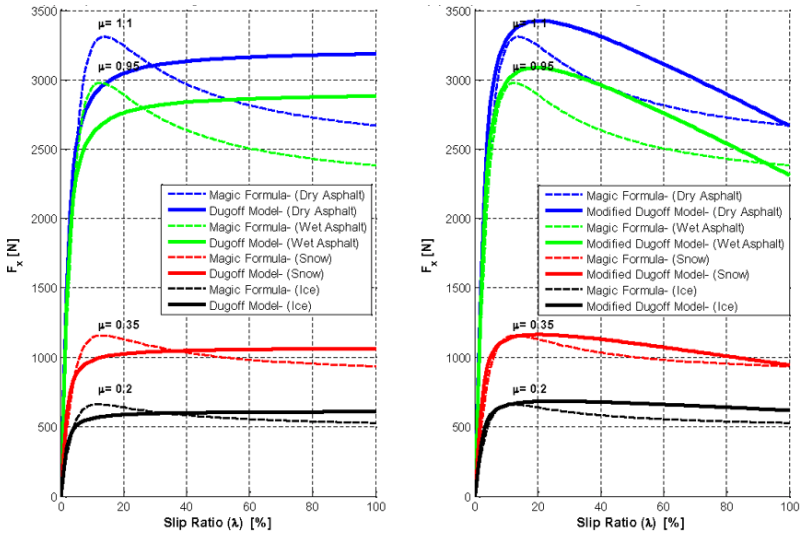

The slip-dependent friction coefficient is expressed as (Ding and Taheri, 2010):

$$\mu_x = \mu_{xp}(1-s) + \mu_{xs} s$$

for pure longitudinal slip, where (44)

$$\mu_{xp} = \frac{c_l}{k_l}\mu$$

$$\mu_{xs} = 0.5545\mu_{xp}^{\ 3} - 0.9697\mu_{xp}^{\ 2} + 1.0424\mu_{xp} \tag{45}$$

where $c_l = 1.125$ and $k_l = 0.925$. c_l and k_l are compensation factor and attenuation factor, respectively. Force calculations based on the modified Dugoff tyre model are shown in Figure 18(b). The results are seen to be coincident to the MF tyre model. The modified Dugoff model has the virtues of the original model, and the precision in nonlinear condition is much improved. Hence, the estimator concept proposed here is

based on the modified Dugoff tyre model. As mentioned previously, the Dugoff model describes the relationship between the tyre force and the slip as a function of two parameters, the tyre stiffness and the tyre to road friction coefficient. In the small slip range, the longitudinal force increases proportional to the slip and the gradient of the force-slip curve is defined as the tyre longitudinal stiffness. Thus, the longitudinal force model in the small-slip range can be expressed as follows:

$$F_x = C_x \cdot \lambda, \quad \text{for} |\lambda| < 3\% \tag{46}$$

Satisfactory performance of the wheel dynamics based observer in the small slip region ($|\lambda| < 3\%$) provides us with an opportunity to adaptively estimate the longitudinal stiffness of the tyre using an online parameter estimation algorithm. Equation (46) can be rewritten into a standard parameter identification form as follows:

$$y(t) = \varphi^T(t) \cdot \theta(t) \tag{47}$$

where $y(t) = F_x$ is the system output (from the wheel dynamics based observer), $(t) = C_x$, is the unknown parameter, and $\varphi^{\mathrm{T}}(t) = \lambda$ is the measured slip ratio. The unknown parameter (t) can be identified in real-time using parameter identification approach. The recursive least squares (RLS) algorithm (Sastry, 1989) provides a method to iteratively update the unknown parameter at each sampling time to minimise the sum of the squares of the modelling error using the past data contained within the regression vector, $\varphi(t)$. The performance of the RLS algorithm is evaluated with simulations where the road surface is designed to have sudden friction coefficient changes, and the vehicle manoeuvre is straight driving with intermittent gas pedal presses.

From Figure 19, it can be see that the estimator shows delayed estimation at the first change due to lack of excitation at that time. Once excitation occurs at 2.2 seconds, the estimator updates the longitudinal stiffness.

Figure 19 (a) road surface condition (bottom) and the tyre slip-ratio (top) during the simulation and (b) longitudinal stiffness estimation result (bottom) and corresponding activation signal (top) (see online version for colours)

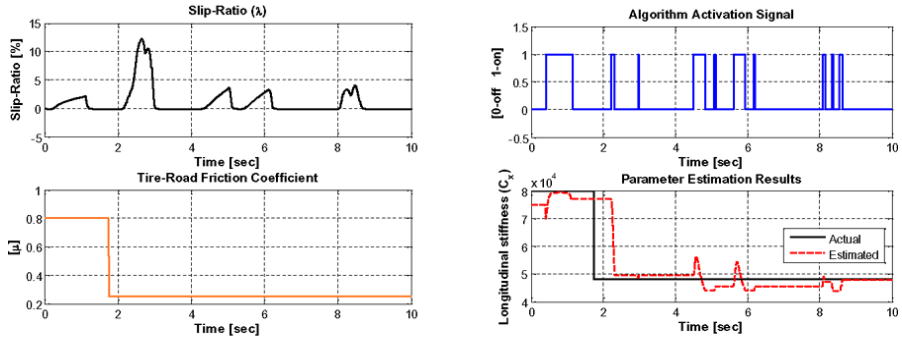

(a) (b)

The second parameter of interest required to describe the relationship between the tyre force and the slip using the Dugoff model is the tyre- road friction coefficient (μ). As

shown previously in Germann et al. (1994), Ray (1997), Gustafsson (1997), Muller et al. (2003), Lee et al. (2004) and Li et al. (2007), there is a co-variation between the friction coefficient and the longitudinal stiffness (C_x) of a tyre. Hence a popular and in many circumstances successful approach to assess the friction is to estimate the longitudinal stiffness, i.e., the incline of the tyre force relative to slip at low slips and from this value distinguishing between different surface conditions.

Contrary to this popular belief**,** some recent studies (Svendenius, 2007) show that the longitudinal stiffness depends on many factors and a generic relation between the slope and the exact friction coefficient is therefore not possible to obtain. The relation is physically difficult to explain and does not always hold. The longitudinal stiffness has been shown to be sensitive to many other factors, namely, tyre inflation pressure, vertical load, wear and temperature, and a change of the stiffness might not guarantee a change in friction. To develop a tyre-road friction coefficient (μ) estimation technique robust against these uncertainties, it is proposed here to use an observer based parameter estimation scheme. The general formulation of the estimation scheme is as follows:

Consider the following nonlinear dynamic system and nonlinear measurement:

$$\begin{aligned} \dot{x} &= f(x,u,\theta) \\ y &= h(x,u,\theta) \end{aligned} \tag{48}$$

where x is the state of the system, y is the measurement, u is the control input, and θ is a vector of constant parameters to be estimated. For the system shown in (61), the following parameter and state estimation algorithm (Friedland, 1997) can be applied:

$$\begin{aligned} \dot{\hat{x}} &= f(\hat{x},\hat{u},\hat{\theta}) + k_1(\hat{x},\hat{u},\hat{\theta})\cdot(y-\hat{y}) \\ \dot{\hat{\theta}} &= k_2(\hat{x},\hat{u},\hat{\theta})\cdot(y-\hat{y}) \end{aligned} \tag{49}$$

Where the observer gains (k_1, k_2) can be determined using an optimisation routine that maximises robust stability against plant uncertainties. Applying the above design methodology for our friction estimation problem, the estimation scheme proposed here is based on equations for the longitudinal motion of the vehicle (Figure 6(a)). The equation of motion can be derived by force equilibrium as shown in Figure 6(a) and the resulting equation is:

$$m\dot{v}_x = \sum F_x - F_{aero\ drag} - F_{grade} - F_{rolling\ resistance} \tag{50}$$

$$\text{or } m\dot{v}_x = \left(F_{x_{fl}} + F_{x_{fr}} + F_{x_{rl}} + F_{x_{rr}}\right) - \frac{1}{2}\rho C_d A_f v_x{}^2 - mg\sin\theta_{grade} - f_r mg\cos\theta_{grade} \tag{51}$$

$$\text{or}\left(F_{x_{fl}} + F_{x_{fr}} + F_{x_{rl}} + F_{x_{rr}}\right) = m\dot{v}_x + \frac{1}{2}\rho C_d A_f v_x{}^2 + mgsin\theta_{grade} + f_r mgcos\theta_{grade} \tag{52}$$

The longitudinal force ($\sum F_x = F_{x_{fl}} + F_{x_{fr}} + F_{x_{rl}} + F_{x_{rr}}$) evolution is modelled with a random walk model, with derivative equal to random noise as:

$$\dot{\hat{F}}_x = 0 \tag{53}$$

Applying principles of sliding mode observer, an estimator can be designed as:

$$\sum \dot{\hat{F}}_x = k_1 \tanh\left(\begin{array}{c}(m\dot{v}_x + \frac{1}{2}\rho C_d A_f v_x^2 + mgsin\theta_{grade} + f_r mgcos\theta_{grade}) \\ -(\hat{F}_{x_{fl}} + \hat{F}_{x_{fr}} + \hat{F}_{x_{rl}} + \hat{F}_{x_{rr}})\end{array}\right) \tag{54}$$

$$\dot{\hat{\mu}} = k_2 \cdot \tanh h\left(\begin{array}{c}(m\dot{v}_x + \frac{1}{2}\rho C_d A_f v_x^2 + mg\sin\theta_{grade} + f_r mg\cos\theta_{grade}) \\ -(\hat{F}_{x_{fl}} + \hat{F}_{x_{fr}} + \hat{F}_{x_{rl}} + \hat{F}_{x_{rr}}) \\ +k_3 \cdot \tanh h(\mu_{C_x} - \hat{\mu})\end{array}\right) \tag{55}$$

Where the system state and parameter to be estimated are $\sum \dot{\hat{F}}_x$ and $\dot{\hat{\mu}}$. $F_{x_{fl,fr,rf,rr}}$ is the longitudinal force estimate for the individual wheels obtained using the modified Dugoff model, updated at each time step using the tyre stiffness and the tyre-road friction coefficient estimate.

The performance of the observer was evaluated with simulations where the road surface is designed to have sudden friction coefficient changes (Table 5).

Table 5 Simulation cases

	Friction coefficient (μ)
Case 1	Low mu
Case 2	Jump mu (high-low-high)

Figure 20 shows that the proposed observer can estimate the longitudinal forces successfully even under high-slip conditions.

2.8.2 Lateral force estimator

A sliding mode observer (SMO) methodology is proposed to observe the tyre lateral forces. The observer estimates lateral forces per axle ($F_{y_{front}}, F_{y_{rear}}$) and then calculates lateral force on each tyre according to the distribution of the estimated vertical forces as:

$$\begin{aligned} F_{y_{fl}} &= \frac{F_{z_{fl}}}{F_{z_{fl}} + F_{z_{fr}}} \times F_{y_{front}} \\ F_{y_{fr}} &= \frac{F_{z_{fr}}}{F_{z_{fl}} + F_{z_{fr}}} \times F_{y_{front}} \\ F_{y_{rl}} &= \frac{F_{z_{rl}}}{F_{z_{rl}} + F_{z_{rr}}} \times F_{y_{rear}} \\ F_{y_{rr}} &= \frac{F_{z_{rr}}}{F_{z_{rl}} + F_{z_{rr}}} \times F_{y_{rear}} \end{aligned} \tag{56}$$

The observer is built in such a way that it requires no tyre force model or prior knowledge of road friction. The tyre forces (axle forces) are modelled with a random walk model:

$$\begin{aligned} \dot{F}_{y_{front}} &= 0 \\ \dot{F}_{y_{rear}} &= 0 \end{aligned} \tag{57}$$

The vehicle dynamics are described by the following state and measurement equations:

$$\begin{aligned} X &= [x_1, x_2, x_3] = [F_{y_{front}}, F_{y_{rear}}, r] \\ Y &= [y_1, y_2] = [a_y, r] \end{aligned} \tag{58}$$

Vectors $\hat{X} = [\hat{x}_1, \hat{x}_2, \hat{x}_3]$ and $\hat{Y} = [\hat{y}_1, \hat{y}_2]$ represent the state and measurement estimations. The measurement model is:

$$\hat{y}_1 = \frac{\hat{x}_1 + \hat{x}_2}{m};\ \hat{y}_{1_1} = \hat{x}_3 \tag{59}$$

where m is the vehicle mass. The estimation errors for states and measurements are denoted respectively as:

$$\begin{aligned} e_x &= [x_1 - \hat{x}_1, x_2 - \hat{x}_2, x_3 - \hat{x}_3] \\ e_y &= [y_1 - \hat{y}_1, y_2 - \hat{y}_2] \end{aligned} \tag{60}$$

The state estimates evolve according to the four-wheel vehicle model, the force model and the sign of the measurement estimation errors as:

$$\begin{aligned} \dot{\hat{x}}_1 &= k_{11} sign(e_{y_1}) + k_{12} sign(e_{y_1}) \\ \dot{\hat{x}}_2 &= k_{21} sign(e_{y_1}) + k_{22} sign(e_{y_2}) \\ \dot{\hat{x}}_3 &= \frac{1}{I_z}\left[a * \hat{x}_2 - b * \hat{x}_1 + \frac{t}{2}((F_{x_{fr}} cos\delta + F_{x_{rr}}) - (F_{x_{fl}} cos\delta + F_{x_{rl}})) \right] + k_{31} sign(e_{y_2}) \end{aligned} \tag{61}$$

where $k_{11}, k_{12}, k_{21}, k_{22}, k_{31}$ are the observer gains. F_{xij} is the longitudinal force estimate for the individual wheels obtained using the estimation scheme proposed in Section 2.8.1.

The force balance equations also include any additional forces and moments generated from longitudinal drive traction or braking forces at the wheels. The longitudinal force terms should be included so the lateral estimation does not become corrupted, especially in situations when the vehicle is undergoing significant acceleration or braking. The drive and traction forces of the front wheels contribute to the lateral force of the steered wheels, and any ESC differential braking produces an additional moment that must be included in the moment equation. A complete study for the convergence of the SMO is presented in (Baffet et al., 2007). The performance of the observer was evaluated for a range of different simulations cases. From Figure 21 we see that the SMO observer produces satisfactory estimations close to the actual value.

Figure 20 Observer performance (ref. Table 5 for a description of the simulation conditions) (see online version for colours)

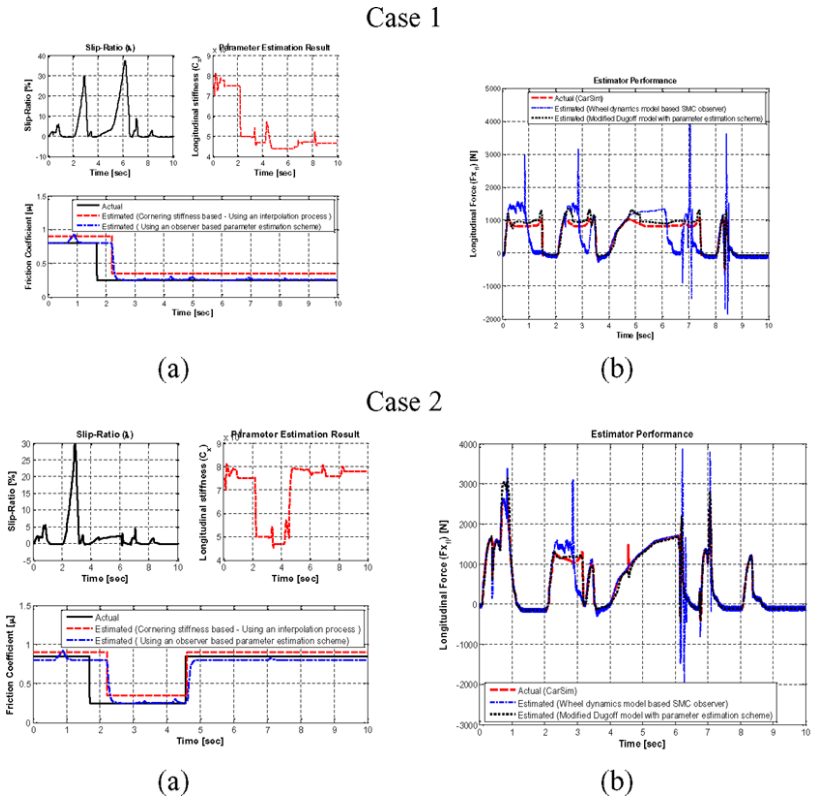

2.9 Vehicle lateral and longitudinal velocity estimator

2.9.1 Estimation concept

Longitudinal and lateral vehicle velocities are important information for active vehicle stability control. But for both technical and economical reasons, these vehicle states cannot be measured directly in a standard car. As a result, the problem of longitudinal and lateral vehicle velocities estimation has attracted considerable attentions of many researchers, and several works have already been conducted over the past few years. Kalman filter based techniques (KF, EKF…) have become a standard technique, used in many nonlinear estimation and machine learning applications. KF is only applied to linear systems, and EKF is developed for state estimation in non-linear systems. But as linearisation of EKF algorithm requires the evaluation of a Jacobian matrix at each time step, the computational complexity is enlarged. To avoid this problem, Julier et al. (1995) proposes Unscented Kalman Filter (UKF) (Wan and Van Der Merwe, 2000), which avoids the linearisation errors and improves filtering accuracy. The UKF acts directly on the nonlinear model and approximates the states by using a set of sigma points, avoiding the linearisation made by the EKF (Julier and Uhlmann, 1997). This study proposes to estimate longitudinal and lateral velocity based on UKF using vehicle dynamics model.

Figure 21 Observer performance: case 1- double lane change, and case 2- slalom steering manoeuvre (55 deg/0.25 Hz) (see online version for colours)

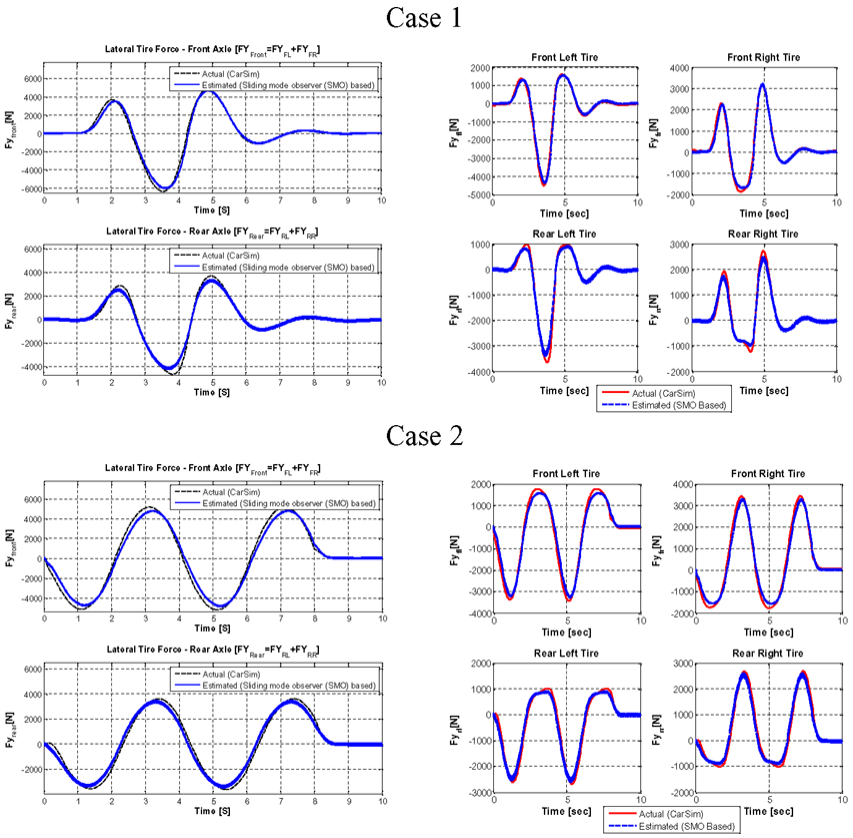

In most vehicle handling and stability studies, two degrees of freedom vehicle model is usually used, which need to make a great linear hypothesis. To obtain a more realistic simulation of vehicle performance, a nonlinear model with four wheels (coupled model very largely used in simulation) is selected in this study. The different equations for the calculation of longitudinal, lateral and yaw motion are as follows:

$$\dot{v_x} = \frac{F_{x_{fl}}\cos\delta + F_{x_{fr}}\cos\delta + F_{x_{rl}} + F_{x_{rr}}}{m}$$

$$+r \cdot v_y - g \cdot \sin(\theta_{pitch}) \tag{62}$$

$$\dot{v_y} = \frac{F_{y_{front}} + F_{y_{rear}}}{m} - r \cdot v_x - g \cdot \sin(\phi_{roll}) \tag{63}$$

$$\dot{r} = \frac{a \cdot F_{y_{front}} - b \cdot F_{y_{rear}} + ((F_{x_{fr}} cos\delta + F_{x_{rr}}) - (F_{x_{fl}} cos\delta + F_{x_{rl}})) \cdot \frac{t}{2}}{I_z} \tag{64}$$

where, m is the vehicle mass; δ is the steering angle of front wheel; a and b are the distances from front and rear axle respectively to center of gravity; t is the vehicle track-width; v_x is longitudinal velocity; v_y is lateral velocity; r is yaw rate; θ_{pitch} is the vehicle pitch (global) angle; ϕ_{roll} is the vehicle roll (global) angle; $F_{x_{ij}}$ are tyre longitudinal forces, and $F_{y_{front}}$ and $F_{y_{rear}}$ are the lateral forces at the front and rear axles, respectively. The nonlinear model can be transformed into standard state-space form with state vector (x) composed of longitudinal speed, lateral speed and yaw rate:

$$x = [v_x, v_y, r] \tag{65}$$

The input vector (u) comprises the measured steering angle, tyre forces (considered estimated beforehand, see Section 2.7), and vehicle global roll and pitch angles (considered estimated beforehand, see Section 2.4):

$$u = [\delta, F_{x_{fl}}, F_{x_{fr}}, F_{x_{rl}}, F_{x_{rr}}, F_{y_{front}}, F_{y_{front}}, \theta_{pitch}, \phi_{roll}] \tag{66}$$

The measure vector (y) comprises vehicle longitudinal velocity (considered estimated beforehand, see Section 2.6), measured yaw rate, and lateral accelerations:

$$y = [v_x, r, a_{y,m}] \tag{67}$$

The process and measurement noise vectors are assumed to be white, zero mean and uncorrelated. The schematic simulation block diagram is represented in Figure 22.

Figure 22 Schematic diagram of the vehicle longitudinal and lateral velocity estimation process (see online version for colours)

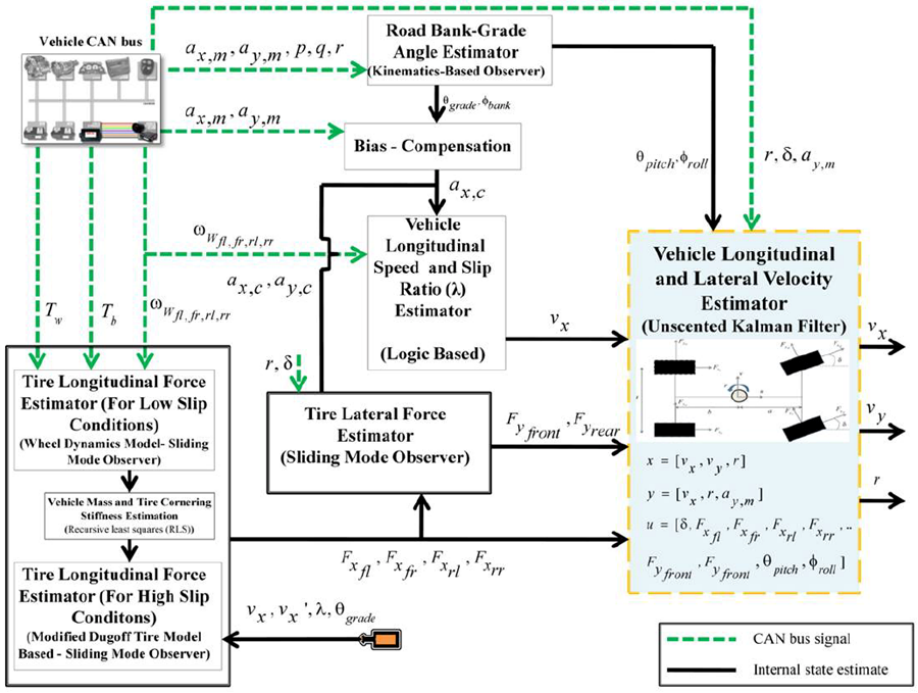

2.9.3 Simulation analysis

The performance of the observer was evaluated for a range of different simulations cases (Table 6 and Figure 23).

Table 6 Simulation cases

	Vehicle speed (Kph)	*Friction coefficient* (μ)	*Test manoeuvre*
Case 1	140	0.85	Double lane change
Case 2	140	Varying (high-low-high)	Double lane change

Figure 23 Observer performance (ref. Table 6 for a description of the simulation conditions) (see online version for colours)

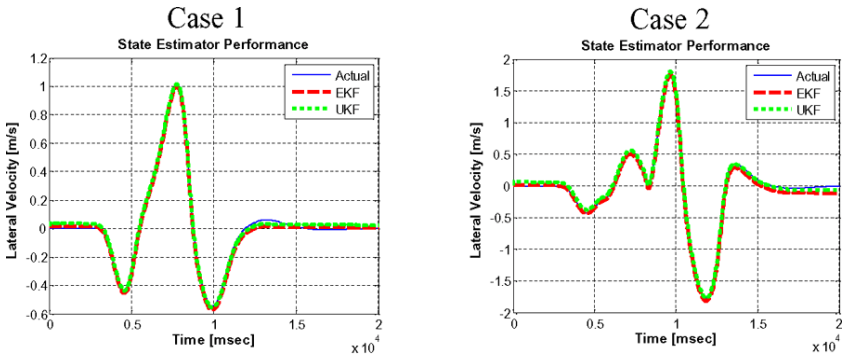

2.10 Tyre slip-ratio and slip-angle estimator

2.10.1 Slip ratio estimator

As shown in Section 2.6, the output of the longitudinal vehicle speed estimation algorithm could also be employed for reliably computing the longitudinal wheel slip. Performance of the observer under extreme braking conditions (Table 7) is demonstrated in Figure 24.

Table 7 Simulation cases

	Vehicle Speed (Kph)	*Friction coefficient (μ)*	*Test manoeuvre*
Case 1	100-0	0.5	Straight-line braking
Case 2	100-0	Varying	Straight-line braking

2.10.2 Slip angle estimator

2.10.2.1 Estimation concept and observer update law

To estimate the tyre slip angle, an update equation for the front slip angle is derived as a function of the tyre forces. A four-wheel vehicle model is employed to simulate the vehicle rigid body dynamic. The dynamic equations of motion of the vehicle model are presented in equations (68)–(70):

$$\dot{v_x} = \frac{F_{x_{fl}}\cos\delta + F_{x_{fr}}\cos\delta + F_{x_{rl}} + F_{x_{rr}}}{m} + r \cdot v_y - g \cdot \sin(\theta_{pitch}) \tag{68}$$

$$\dot{v_y} = \frac{F_{y_{front}} + F_{y_{rear}}}{m} - r \cdot v_x - g \cdot \sin(\phi_{roll}) \tag{69}$$

$$\dot{r} = \frac{\begin{array}{c} a \cdot F_{y_{front}} - b \cdot F_{y_{rear}} + ((F_{x_{fr}} cos\delta + F_{x_{rr}}) \\ -(F_{x_{fl}} cos\delta + F_{x_{rl}})) \cdot \frac{t}{2} \end{array}}{I_z} \tag{70}$$

where $F_{y_{front}} = (F_{y_{fl}}\cos\delta + F_{x_{fl}}\sin\delta) + (F_{y_{fr}}\cos\delta + F_{x_{fr}}\sin\delta)$ and $F_{y_{rear}} = F_{y_{rl}} + F_{y_{rr}}$ are the lateral forces at the front and rear axles, respectively.

Using kinematics, the front and rear tyre slip angles are linearised to be:

$$\alpha_f = \frac{v_y + a \cdot r}{v_x} - \delta \tag{71}$$

$$\alpha_r = \frac{v_y - b \cdot r}{v_x} \tag{72}$$

The update equation for the front slip angle is derived by taking the derivative of (72)

$$\dot{\alpha_f} = \frac{\dot{v_y} + a \cdot \dot{r}}{v_x} - \dot{\delta} \tag{73}$$

Substituting expressions for $\dot{v_y}$ (equation (69)), and $\dot{r}$ (equation (70)) in equation (73), we get:

$$\dot{\alpha_f} = \frac{\begin{array}{c} \left(\frac{F_{y_{front}} + F_{y_{rear}}}{m} - r \cdot v_x\right) \\ + a \cdot \left(\begin{array}{c} a \cdot F_{y_{front}} - b \cdot F_{y_{rear}} + ((F_{x_{fr}} cos\delta + F_{x_{rr}}) \\ -(F_{x_{fl}} cos\delta + F_{x_{rl}})) \cdot \frac{t}{2} \end{array} \right) \\ \frac{I_z}{} \end{array}}{v_x} - \dot{\delta} \tag{74}$$

Rearranging above equation, we get:

$$\dot{\alpha_f} = \left(\frac{1}{mv_x} + \frac{a^2}{I_z v_x}\right) \cdot F_{y_{front}} + \left(\frac{1}{mv_x} - \frac{ab}{I_z v_x}\right) \cdot F_{y_{rear}}$$
$$+ \frac{t \cdot a}{2I_z v_x}((F_{x_{fr}} cos\delta + F_{x_{rr}}) - (F_{x_{fl}} cos\delta + F_{x_{rl}})) - r - \dot{\delta} \tag{75}$$

Figure 24 Observer performance (ref. Table 7 for a description of the simulation conditions) (see online version for colours)

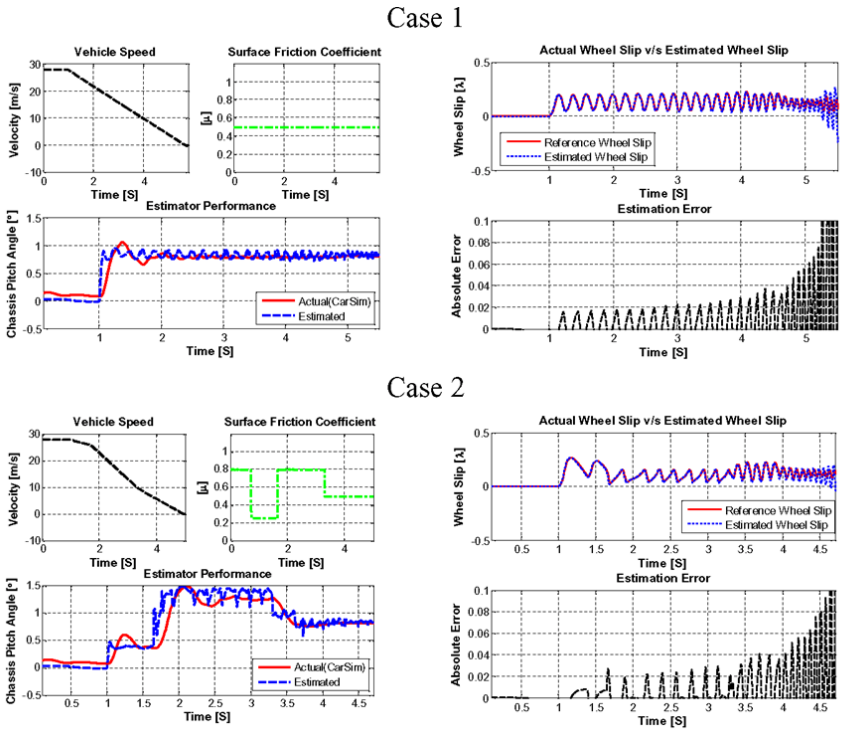

Thus, to update $\dot{\hat{\alpha}}_f$, we may integrate the following observer update law:

$$\dot{\hat{\alpha}}_f = \left(\frac{1}{mv_x} + \frac{a^2}{I_z v_x}\right) \cdot F_{y_{front}}$$
$$+ \left(\frac{1}{mv_x} - \frac{ab}{I_z v_x}\right) \cdot F_{y_{rear}}$$
$$+ \frac{t \cdot a}{2I_z v_x}\left(\left(F_{x_{fr}} \cos\delta + F_{x_{rr}}\right) - \left(F_{x_{fl}} \cos\delta + F_{x_{rl}}\right)\right) - r - \dot{\delta}$$
$$+ k(ma_y - F_{y_{front}} - F_{y_{rear}}) \tag{76}$$

where k is the observer feedback gain and a_y is the measured lateral acceleration. Once $\hat{\alpha}_f$ is updated, the rear slip angle estimate ($\hat{\alpha}_r$) can be updated using the kinematic relationship described by equation (72).

From equation (76), we can see that an estimate of the tyre slip angle can be made, provided we have real-time information about the tyre longitudinal/lateral forces. To successfully achieve the objective of estimating the tyre slip angle, an integrated estimation scheme is proposed (Figure 25). The estimation scheme consists of two key blocks:

- tyre longitudinal force estimator
- tyre lateral force estimator.

2.10.2.2 *Slip angle estimator performance*

Using the tyre longitudinal/lateral force estimates (considered estimated beforehand, see Section 2.8), the performance of the slip angle observer (equation (86)) was evaluated for range of different aggressive steering manoeuvres. Figure 26 shows that the proposed observer can estimate the tyre slip angle successfully even for challenging (aggressive manoeuvring) operating conditions.

Figure 25 Schematic diagram of the tyre slip angle estimation process (see online version for colours)

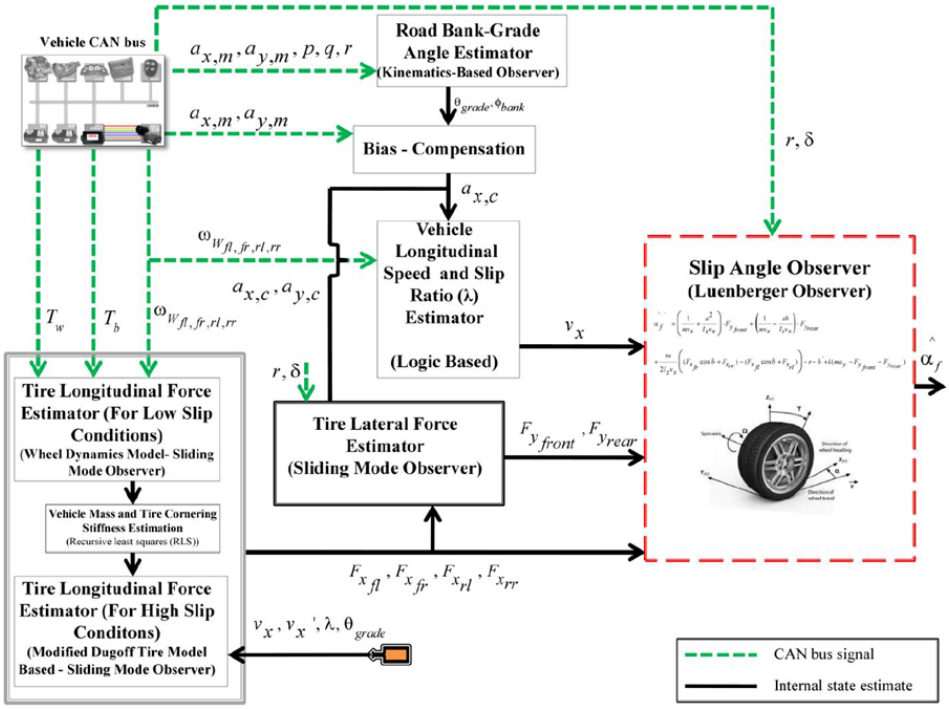

Figure 26 Observer performance – slalom steering manoeuvre (55 deg/0.25 Hz) (see online version for colours)

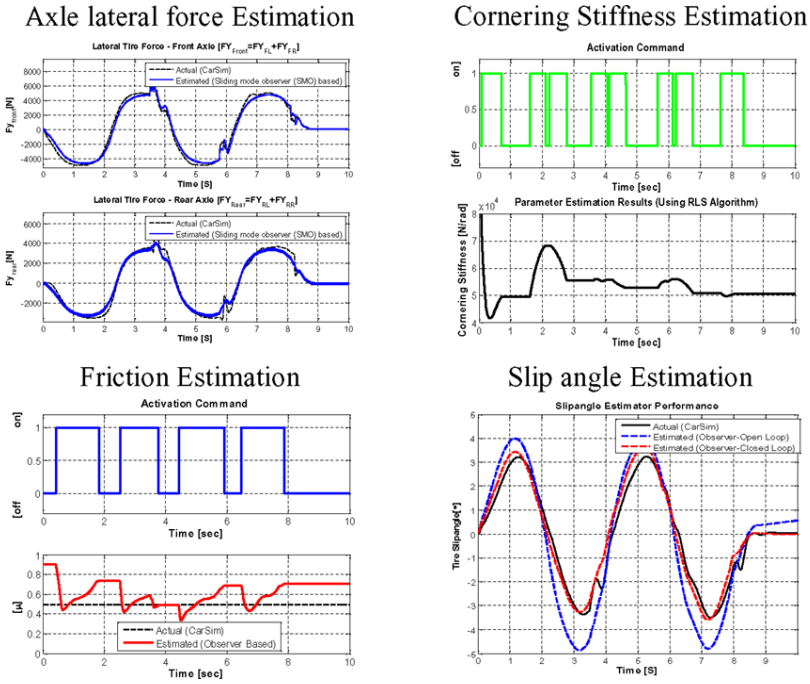

3 Conclusion

Active safety systems such as the antilock braking system (ABS), traction control system (TCS) or Electronic Stability Program (ESP) intervene before a crash occurs and significantly contribute to the reduction in the number of crashes. For the future development trend of these systems, a more complex and integrated control unit requires additional information about the vehicle dynamics. Some fundamental parameters such as tyre forces and sideslip angle are effective in describing vehicle dynamics, however, a direct measurement of these variables is cost-prohibitive for automotive applications. This study presents a method to estimate these parameters of interest using observer technologies. The proposed observer consists of an integrated vehicle state estimator comprising of a series of model based and kinematic based observers arranged in a cascaded structure. It is assumed that a set of data obtained from a low-cost six-dimensional inertial measurement unit is available. This includes the linear acceleration of the vehicle and the angular rates of all axes. In addition, the observer exploits the data from the wheel speed sensors and the steering-wheel angle, which are already available for recent production cars. The estimator is implemented in the Matlab/Simulink and CarSim® software environment. Results presented here show the ability of cascaded estimators to provide accurate estimates of vehicle states.

The main contribution of this work is to estimate tyre forces and sideslip angle with an acceptable accuracy using standard sensors which are available in most of the series production vehicles today. Therefore, this method enables a cost-effective

implementation for future real-time vehicle applications. The longitudinal/lateral tyre forces provide important information on the computation of the optimised active longitudinal and lateral tyre forces to be generated by the different control modules of an integrated chassis control system typically consisting of individual modular chassis control systems such as the ESC, active front steering (AFS) and continuous damping control (CDC). An integrated chassis control ensures optimal tyre usage via an optimum longitudinal and lateral tyre force distribution by four-wheel independent steering, driving, and braking. Using an integrated state estimation approach also gives added value in terms of more information, increased robustness and the opportunity to reduce costs by allowing the use of fewer or lower resolution sensors.

These improved state estimates can be used to develop a more reliable and efficient vehicle stability control algorithm. It is expected that a new control strategy aiming to use all the information available from the vehicle state estimator would significantly enhance vehicle stability during emergency evasive manoeuvres on various road conditions ranging from dry asphalt to very slippery packed snow road surfaces. Another potential advantage could be in terms of minimising false ESC interventions. In a situation where an ESC is tuned to prioritise stability over handling for robustness reasons, brake interventions may come too early and feel harsh to the driver. However, with knowledge of the sideslip angle, the control engineer has more freedom to tune the ESC intervention thresholds and prevent brake interventions occurring too early. It is noteworthy to mention that the vehicle state information derived either from chassis mounted accelerometer sensors or from engine/brake torque information are fraught with reliability problems. The development of a sensorised smart/intelligent tyre system (Singh et al., 2012, 2013; Morinaga, 2013; Yasushi Hanatsuka and Morinaga, 2013; Arat et al., 2013, 2014; Singh and Taheri, 2015) is expected to eliminate some of the vehicle sensors and provide accurate, reliable and real-time information about magnitudes, directions and limits of force for each tyre. Future work will explore the possibility of developing novel sensor signal fusion schemes combining the tyre sensed information from an intelligent tyre and vehicle sensor information available on typical passenger cars to further improve the accuracy of the vehicle state estimator.

References

Arat, M.A., Singh, K.B. and Taheri, S. (2013) 'Optimal tire force allocation by means of smart tire technology', *SAE International Journal of Passenger Cars-Mechanical Systems*, Vol. 6, No. 2013–1–694, pp.163–176.

Arat, M.A., Singh, K.B. and Taheri, S. (2014) 'An intelligent tyre based adaptive vehicle stability controller', *International Journal of Vehicle Design*, Vol. 65, Nos. 2–3, pp.118–143.

Baffet, G., Charara, A. and Lechner, D. (2007) 'Experimental evaluation of a sliding mode observer for tire-road forces and an extended Kalman filter for vehicle sideslip angle', *2007 IEEE*, pp.3877–3882.

Baffet, G., Charara, A. and Lechner, D. (2008) 'Estimation of tire-road forces and vehicle sideslip angle', *Advances in Robotics, Automation and Control*, InTech.

Baffet, G., Charara, A. and Lechner, D. (2009) 'Estimation of vehicle sideslip, tire force and wheel cornering stiffness', *Control Engineering Practice*, Vol. 17, No. 11, pp.1255–1264.

Bishop, G. (2006) *An Introduction to the Kalman Filter*.

Chen, B-C. and Hsieh, F-C. (2008) 'Sideslip angle estimation using extended kalman filter', *Vehicle System Dynamics*, 46 (S1): 353–364.

Chen, S-K., Moshchuk, N., Nardi, F. and Ryu, J. (2010) 'Vehicle rollover avoidance', *IEEE Control Systems*., Vol. 30, No. 4, pp.70–85.

Cheng, Q., Correa-Victorino, A. and Charara, A. (2011) 'A new nonlinear observer using unscented Kalman filter to estimate sideslip angle, lateral tire road forces and tire road friction coefficient', *2011 IEEE*, pp.709–714.

Cho, K., Son, H., Choi, S.B. and Kang, S. (2010) 'Lateral acceleration compensation of a vehicle based on roll angle estimation', *2010 IEEE*, pp.1363–1368.

Cho, W., Yoon, J., Yim, S., Koo, B. and Kyongsu, Y (2010) 'Estimation of tire forces for application to vehicle stability control', *IEEE Transactions on Vehicular Technology*, Vol. 59, No. 2, pp.638–649.

Chu, L., Shi, Y., Zhang, Y., Liu, H. and Xu, M. (2010) 'Vehicle lateral and longitudinal velocity estimation based on unscented Kalman filter', *2010 IEEE*, pp.V3–427.

Chu, L., Chao, L.B., Zhang, Y. and Shi, Y. (2011) 'Design of longitudinal vehicle velocity observer using fuzzy logic and Kalman filter', *2011 IEEE*, pp.3225–3228.

Dakhlallah, J., Glaser, S., Mammar, S. and Sebsadji, Y. (2008) 'Tire-road forces estimation using extended kalman filter and sideslip angle evaluation', *2008 IEEE*, pp.4597–4602.

De Bruyne, S., Van Der Auweraer, H. and Anthonis, J. (2011) *Advanced State Estimator Design for an Active Suspension*.

Ding, N. and Taheri, S. (2010) 'A modified dugoff tire model for combined-slip forces', *Tire Science and Technology*, Vol. 38, No. 3, pp.228–244.

Doumiati, M., Victorino, A., Charara, A., Baffet, G. and Lechner, D. (2008) 'An estimation process for vehicle wheel-ground contact normal forces', *IFAC Proceedings Volumes*, Vol. 41, No. 2, pp.7110–7115.

Doumiati, M., Victorino, A.C., Charara, A. and Lechner, D. (2011b) 'Onboard real-time estimation of vehicle lateral tire–road forces and sideslip angle', *IEEE/ASME Transactions on Mechatronics*, Vol. 16, No. 4, pp.601–614.

Doumiati, M., All Charara, A.V. and Lechner, D. (2009a) 'Lateral load transfer and normal forces estimation for vehicle safety: experimental test', *Vehicle System Dynamics*, Vol. 47, No. 12, pp.1511–1533.

Doumiati, M., All Charara, A.V. and Lechner, D. (2009b) 'Estimation of vehicle lateral tire-road forces: a comparison between extended and unscented Kalman filtering', *2009 IEEE*, pp.4804–4809.

Doumiati, M., All Charara, A.V. and Lechner, D. (2009c) 'Unscented Kalman filter for real-time vehicle lateral tire forces and sideslip angle estimation', *2009 IEEE*, pp.901–906.

Doumiati, M., All Charara, A.V. and Lechner, D. (2009d) *Virtual Sensors, Application to Vehicle Tire-Road Normal Forces for Road Safety*, 2009 IEEE, pp.3337–3343.

Doumiati, M., All Charara, A.V. and Lechner, D. (2010a) 'Observers for vehicle tyre/road forces estimation: experimental validation', *Vehicle System Dynamics*, Vol. 48, No. 11, pp.1345–1378.

Doumiati, M., Victorino, A., Charara, A. and Lechner, D. (2010b) 'A method to estimate the lateral tire force and the sideslip angle of a vehicle: experimental validation', *2010 IEEE*, pp.6936–6942.

Doumiati, M., Victorino, A., Charara, A. and Lechner, D. (2011a) 'Estimation of road profile for vehicle dynamics motion: experimental validation', *2011 IEEE*, pp.5237–5242.

Eric Tseng, H., Xu, L. and Hrovat, D. (2007) 'Estimation of land vehicle roll and pitch angles', *Vehicle System Dynamics*, Vol. 45, No. 5, pp.433–443.

Fatnyi, H.K., Kang, D. and Stein, J.L. (2008) 'Online vehicle mass estimation using recursive least squares and supervisory data extraction', *2008 IEEE*, pp.1842–1848.

Friedland B. (1997) 'A nonlinear observer for estimating parameters in dynamic systems', *Automatica*, Vol. 33, No. 8, pp.1525–1530.

Germann, S., Wurtenberger, M. and Daiss, A. (1994) 'Monitoring of the friction coefficient between tyre and road surface', pp.613–618.

Ghandour, R., Victorino, A., Doumiati, M. and Charara, A. (2010) 'Tire/road friction coefficient estimation applied to road safety', *2010 IEEE*, pp.1485–1490.

Ghandour, R., da Cunha, F.H.R., Victorino, A., Charara, A. and Lechner, D. (2011) 'Risk indicators prediction based on the estimation of tire/Road forces and the maximum friction coefficient: experimental validation', *2011 IEEE*, pp.700–705.

Ghandour, R., Victorino, A., Charara, A.N. and Lechner, D. (2011) 'A vehicle skid indicator based on maximum friction estimation', *IFAC Proceedings Volumes*, Vol. 44, No. 1, pp.2272–2277.

Greenwood, D.T. (1988) *Principles of Dynamics*, 2nd ed., Prentice Hall, New Jersey.

Grip, H.F., Imsland, L., Johansen, T.A., Kalkkuhl, J.C. and Suissa, A. (2009a) 'Estimation of road inclination and bank angle in automotive vehicles', *2009 IEEE*, pp.426–432.

Grip, H.F., *et al.* (2009b) 'Vehicle sideslip estimation', *IEEE Control Systems*, Vol. 9, No. 5).

Gustafsson, F. (1997) 'Slip-based tire-road friction estimation', *Automatica*, Vol. 33, No. 6, pp.1087–1099.

Hac, A., Brown, T. and Martens, J. (2004) *Detection of Vehicle Rollover*.

Hac, A., Nichols, D. and Sycjnarowicz, D. (2010) *Estimation of Vehicle Roll Angle and Side Slip for Crash Sensing*.

Hernandez-Alcantara, D., Amezquita-Brooks, L. and Morales-Menendez, R. (2014) *State-Observers for Semi-Active Suspension Control Applications with Low Sensitivity to Unknown Road Surfaces*.

Hong, K-S. and Park, S. (2010) 'Road-frequency adaptive control for semi-active suspension systems', *International Journal of Control, Automation and Systems*, Vol. 8, No. 5, pp.1029–1038.

Hoseinnezhad, R. and Bab-Hadiashar, A. (2011) 'Efficient antilock braking by direct maximization of tire–road frictions', *IEEE Transactions on Industrial Electronics*, Vol. 58, No. 8, pp.3593–3600.

Hsiao, T., Liu, N.C. and Chen, S.Y. (2011) *Robust Estimation of the Friction Forces Generated by Each Tire of a Vehicle*, 2011 IEEE, pp.5261–5266.

Hsu, Y-H. J., Laws, S.M. and Christian Gerdes, J. (2010) 'Estimation of tire slip angle and friction limits using steering torque', *IEEE Transactions on Control Systems Technology*, Vol. 18, No. 4, pp.896–907.

Hu, L., Shi, Y., Zhang, Y., Liu, H. and Xu, M. (2010) *Vehicle Lateral and Longitudinal Velocity Estimation Based on Adaptive Kalman Filter*, pp.325–329.

Jiang, F. and Gao, Z. (2000) *An Adaptive Nonlinear Filter Approach to the Vehicle Velocity Estimation for ABS*, IEEE, pp.490–495.

Julier, S.J. and Uhlmann, J.K. (1997) *New Extension of the Kalman Filter to Nonlinear Systems*, 1997 International Society for Optics and Photonics, pp.182–194.

Julier, S.J., Uhlmann, J.K. and Durrant-Whyte, H.F. (1995) *A New Approach for Filtering Nonlinear Systems*, IEEE, pp.1628–1632.

Kaldas, M.M.S., Çalışkan, K., Henze, R. and Küçükay, F. (2011) 'Development of a semi-active suspension controller using adaptive-Fuzzy with kalman filter', *SAE International Journal of Materials and Manufacturing*, Vol. 4(2011–1–431), pp.505–515.

Klein, R., Daiss, A. and Eichfeld, H. (1996) *Antilock Braking System and Vehicle Speed Estimation Using Fuzzy Logic*, 1996.

Kobayashi, K., Cheok, K.C. and Watanabe, K. (1995) *Estimation of Absolute Vehicle Speed Using Fuzzy Logic Rule-Based Kalman Filter*, IEEE, pp.3086–3090.

Koch, G., Kloiber, T., Pellegrini, E. and Lohmann, B. (2010) *A Nonlinear Estimator Concept for Active Vehicle Suspension Control*, 2010 IEEE, pp.4576–4581.

Lee, C., Hedrick, K.and Yi, K. (2004) 'Real-time slip-based estimation of maximum tire-road friction coefficient', *IEEE/ASME Transactions on Mechatronics*, Vol. 9, No. 2, pp.454–458.

Li, K., Misener, J.A. and Hedrick, K. (2007) 'On-board road condition monitoring system using slip-based tyre-road friction estimation and wheel speed signal analysis', *Proceedings of the Institution of Mechanical Engineers, Part K: Journal of Multi-Body Dynamics*, Vol. 221, No. 1, pp.129–146.

M'sirdi, N.K., Rabhi, A., Ouladsine, M. and Fridman, L. (2006) *First and High-Order Sliding Mode Observers to Estimate the Contact Forces*, 2006 IEEE, pp.274–279.

Masmoudi, R. and Hedrick, J. (1992) 'Estimation of vehicle shaft torque using nonlinear observers', *Journal of Dynamic Systems, Measurement and Control*, Vol. 114, No. 3, pp.394–400.

Morinaga, H. (2013) 'CAIS technology for detailed classification of road surface condition', *Proceedings of the Tire Technology Expo*, Cologne, Germany, pp.5–7.

Muller, S., Uchanski, M. and Hednck, K. (2003) 'Estimation of the maximum tire-road friction coefficient', *Journal of Dynamic Systems, Measurement and Control*, Vol. 125, No. 4, pp.607–617.

Nam, K., Oh, S., Fujimoto, H. and Hori, Y. (2011) *Vehicle State Estimation for Advanced Vehicle Motion Control Using Novel Lateral Tire Force Sensors*, 2011 IEEE, pp.4853–4858.

Oh, J. and Choi, S.B. (2011) *Design of a New Composite Observer for Vehicle Velocity and Attitude Estimation*, 2011 p.

Pan, Z., Zong, C., Zhang, J., Xie, X. and Dong, Y. (2009) *UKF and EKF Estimator Design Based on a Nonlinear Vehicle Model Containing UniTire Model*, 2009 IEEE, pp.4780–4784.

Park, J.l., Yoon, J.Y., Kirn, D.S. and Yi, K.S. (2008) 'Roll state estimator for rollover mitigation control', *Proceedings of the Institution of Mechanical Engineers, Part D: Journal of Automobile Engineering*, Vol. 222, No. 8, pp.1289–1312.

Pletschen, N. and Badur, P. (2014) 'Nonlinear state estimation in suspension control based on takagi-sugeno model', *IFAC Proceedings Vols*, Vol. 47, No. 3, p.11231–11237.

Rabhi, A., M'sirdi, N.K. and Elhajjaji, A. (2007) *Estimation of Contact Forces and Tire Road Friction*, 2007 IEEE, pp.1–6.

Rajamani, R., Piyabongkarn, D., Tsourapas, V. and Lew, J.Y. (2009) *Real-Time Estimation of Roll Angle and CG Height for Active Rollover Prevention Applications*, 2009 IEEE, pp.433–438.

Rajamani, R., Piyabongkarn, D., Tsourapas, V. and Lew, J.Y. (2011) 'Parameter and state estimation in vehicle roll dynamics', *IEEE Transactions on Intelligent Transportation Systems*, Vol. 12, No. 4, pp.1558–1567.

Rajamani, R., Phanomchoeng, G., Piyabongkarn, D. and Lew, J.Y. (2012) 'Algorithms for real-time estimation of individual wheel tire-road friction coefficients', *IEEE/ASME Transactions on Mechatronics*, Vol. 17, No. 6, pp.1183–1195.

Rath, J.J., Veluvolu, K.C. and Defoort, M. (2014) 'Adaptive super-twisting observer for estimation of random road excitation profile in automotive suspension systems', *The Scientific World Journal*.

Ray, L.R. (1995) 'Nonlinear state and tire force estimation for advanced vehicle control', *IEEE Transactions on Control Systems Technology*, Vol. 3, No. 1, pp.117–124.

Ray, L.R. (1997) 'Nonlinear tire force estimation and road friction identification: simulation and experiments1, 2', *Automatica*, Vol. 33, No. 10, pp.1819–1833.

Rehm, A. (2010) *Estimation of Vehicle Roll Angle*, 2010 IEEE, pp.1–4.

Ryu, J., Moshchuk, N.K. and Chen, S-K. (2007) *Vehicle State Estimation for Roll Control System*, 2007 IEEE, pp.1618–1623.

Samadi, B., Kaiemi, R., Nikravesh, K.Y. and Kabganian, M. (2001) *Real-Time Estimation of Vehicle State and Tire-Road Friction Forces*, 2001 IEEE, pp.3318–3323.

Sastry, S. (1989) 'Adaptive control; stability', *Convergence and Robustness*, pp.139–140.

Sebsadji, Y., Glaser, S., Mammar, S. and Dakhlallah, J. (2008) *Road Slope and Vehicle Dynamics Estimation*, 2008 IEEE, pp.4603–4608.

Singh, K.B. and Taheri, S. (2015) 'Estimation of tire–road friction coefficient and its application in chassis control systems', *Systems Science and Control Engineering*, Vol. 3, No. 1, pp.39–61.

Singh, K.B., Arat, M.A. and Taheri, S. (2012) 'Enhancement of collision mitigation braking system performance through real-time estimation of tire-road friction coefficient by means of smart tires', *SAE International Journal of Passenger Cars-Electronic and Electrical Systems*, Vol. 5, No. 2012–01–2014, pp.607–624.

Singh, K.B., Arat, M.A. and Taheri, S. (2013) 'An intelligent tire based tire-road friction estimation technique and adaptive wheel slip controller for antilock brake system', *Journal of Dynamic Systems, Measurement and Control*, Vol. 135, No. 3, p.031002.

Svendenius, J. (2007) *Tire Modeling and Friction Estimation*, PhD Theses.

Tanelli, M., Savaresi, S.M. and Cantoni, C. (2006) *Longitudinal Vehicle Speed Estimation for Traction and Braking Control Systems*, 2006 IEEE, pp.2790–2795.

Tseng, H.E. (2001) 'Dynamic estimation of road bank angle', *Vehicle System Dynamics*, Vol. 36, Nos. 4–5, pp.307–328.

Tsourapas, V., Piyabongkarn, D., Williams, A.C. and Rajamani, R. (2009) *New Method of Identifying Real-Time Predictive Lateral Load Transfer Ratio for Rollover Prevention Systems*, 2009 IEEE, pp.439–444.

Vahidi, A., Stefanopoulou, A. and Peng, H. (2005) 'Recursive least squares with forgetting for online estimation of vehicle mass and road grade: theory and experiments', *Vehicle System Dynamics*, Vol. 43, No. 1, pp.31–55.

Wan, E.A. and Van Der Merwe, R. (2000) *The Unscented Kalman Filter for Nonlinear Estimation*, 2000 IEEE, pp.153–158.

Watanabe, K., Kobayashi, K. and Cheok, K.C. (1992) *Absolute Speed Measurement of Automobile From Noisy Acceleration and Erroneous Wheel Speed Information*.

Yasushi Hanatsuka, Y. and Morinaga, H. (2013) *Method for Estimating Condition of Road Surface* (*US 20130116*972 *A1*): USA Patent.

Yi, K., Yoon, J. and Kim, D. (2007) *Model-Based Estimation of Vehicle Roll State for Detection of Impending Vehicle Rollover*, 2007 IEEE, pp.1624–1629.

Zhang, W., Ding, N., Yu, G. and Zhou, W. (2009) *Virtual Sensors Design in Vehicle Sideslip Angle and Velocity of the Centre of Gravity Estimation*, 2009 IEEE, pp.3–652.

Zhu, T. and Zheng, H. (2008) *Application of Unscented Kalman Filter to Vehicle State Estimation*, 2008 IEEE, pp.135–139.

Nomenclature

In this section all symbols used in this work are listed.

Fy_f	Front axle lateral force (in vehicle body axis)
Fy_r	Rear axle lateral force (in vehicle body axis)
$\sum Fx$	Summation of tire longitudinal forces (in vehicle body axis)
ϕ	Roll angle
θ:	Pitch angle
ψ	Yaw angle

v_x :	Longitudinal velocity at C.G
v_y	Lateral velocity at C.G
a_x	Longitudinal acceleration measured at C.G
a_y	Lateral acceleration measured at C.G
a_z	Vertical acceleration measured at C.G
p	Roll rate measured at C.G
q	Pitch rate measured at C.G
r	Yaw rate measured at C.G
m	Total vehicle mass
m_s	Sprung mass of the vehicle
m_u	Unsprung mass of the vehicle
g	Gravitational constant
h_{cg}	Vehicle C.G. height
h_r	Eight of the roll center from the ground
$h_{r_{front}}$	Height of the front roll center from the ground
$h_{r_{rear}}$	Height of the rear roll center from the ground
h_a	Height of the unsprung mass from the ground
h_{roll}	Height of the sprung mass from the roll axis
a	Distance between C.G.and frontaxle
b	Distance between C.G.and rearaxle
L	Distance between front and rear axle
I_z	Moment of inertia about z-axis/yaw axis
I_x	Moment of inertia about x-axis/roll axis
β	Vehicle sideslip angle
δ_{sus}	Suspension deflection
λ	Tyre slip-ratio
α	Tyre slip-angle
T_e	Engine torque
T_b	Brake torque
T_w	Wheel torque
	Wheel angular speed

ω_w	Angular position of the wheel
k_{roll}	Roll stiffness
c_{roll}	Roll damping coefficient
$\phi_{chassis}$	Vehicle chassis roll angle
$\theta_{chassis}$	Vehicle chassis pitch angle
$\phi_{road\ bank}$	road bank angle
$\theta_{road\ grade}$	Road grade angle
t	Track width
$\phi_{vehicle\ roll}$	Vehicle roll angle
$\phi_{vehicle\ roll_{SS}}$	Vehicle steady state roll angle
$\phi_{vehicle\ roll_{TS}}$	Vehicle transient state roll angle
$\theta_{vehicle\ pitch}$	Vehicle pitch angle
$\theta_{vehicle\ pitch_{SS}}$	Vehicle steady state pitch angle
$\phi_{vehicle\ pitch_{TS}}$	Vehicle transient state pitch angle
$a_{x,m}$	Measured longitudinal acceleration of the vehicle
$a_{y,m}$	Measured lateral acceleration of the vehicle
$a_{x,c}$	Bias compensated longitudinal acceleration of the vehicle
$a_{y,c}$	Bias compensated lateral accelerationof the vehicle
r_o	Originial wheel radius
r_w	Effective wheel radius
v_w	Linear velocity of the four wheels
$v_{average}$	Average of the four wheel speeds
$v_{non-driven\ average}$	Average of the two non-driven wheel speeds
v_{min} :	Vehile speed threshold
a_{acc}	Acceleration threshold
a_{dcc}	Decceleration threshold
$Fz_{front\ axle}$	Normal force of the frontaxle
$Fz_{rear\ axle}$	Normal force of the rear axle

Fx_{fl}	Longitudinal force of the front-leftwheel
Fx_{fr}	Longitudinal force ofthe front-rightwheel
Fx_{rl}	Longitudinal force ofthe rear-leftwheel
Fx_{rr}	Longitudinal force of the rear-rightwheel
Fy_{fl}	Lateral force of the front-leftwheel
Fy_{fr}	Lateral force of the front-rightwheel
Fy_{rl}	Lateral force of the rear-leftwheel
Fy_{rr}	Lateral force of the rear-rightwheel
Fz_{fl}	Vertical force of the front-leftwheel
Fz_{fr}	Vertical force of the front-rightwheel
Fz_{rl}	Vertical force of the rear-leftwheel
Fz_{rr}	Vertical force ofthe rear-rightwheel
F_{rr}	Rolling resistance force
$W_{Lateral\ Load\ Transfer}$	Vehicle lateral load transfer
$W_{Longitudinal\ Load\ Transfer}$	Vehicle longitudinal load transfer
LTR	Load transfer ratioδ
k_f	Front suspension stiffness
k_r	Rear suspension stiffness
k_{bf}	Brake gain of the frontwheel
k_{br}	Brake gain of the rearwheel
J_w	Spin inertia for each wheel
k_t	Spring ratio of the tire
δ	Tyre steer angle
C_x	Tyre longitudinal stiffness
C_y	Tyre cornering stiffness
μ	Tyre road friction coefficient
C_d	Vehicle drag coefficient
A_f	Frontal area of the vehicle
ρ	Density of air

A	State matrix
B	Input matrix
C	Output matrix
D	Feedthrough matrix
P	Covariance matrix

Appendix

In this appendix section, the effectiveness of the overall integrated scheme is validated for a double lane change manoeuvre.

List of vehicle model parameters used in simulation:

$m = 1570$	Total mass of the vehicle (kg)
$m_s = 1370$	Sprung mass of the vehicle (kg)
$I_z = 4192$	Moment of inertia about the yaw axis (kg-m^2)
$a = 1.11$	Distance from the CG to the front axle (m)
$b = 1.66$	Distance from the CG to the rear axle (m)
$t_r = 1.6$	Track width (m)
Steering gear ratio	17.25
$h_r = 0.42$	Height of the roll center (m)
$h_a = 0.3$	Unsprung mass from the ground (m)
$h_s = 0.11$	CG to roll center distance (m)
$h_{cg} = h_r + h_s$	CG height from ground (m)
$k_{sf} = 29.661$	Front suspension spring stiffness (N/mm)
$k_{sr} = 20.082$	Rear suspension spring stiffness (N/mm)
$k_{roll} = 29$	Roll stiffness (N-m/deg)